Zhang, Zhibo, David B. Mechem, J. Christine Chiu, and Justin A. Covert. “A Comprehensive Analysis of Uncertainties in Warm Rain Parameterizations in Climate Models Based on in Situ Measurements.” Journal of the Atmospheric Sciences 1, no. aop (May 13, 2024). https://doi.org/10.1175/JAS-D-23-0198.1.

https://doi.org/10.1175/JAS-D-23-0198.1

A comprehensive analysis of uncertainties in warm rain parameterizations in climate models based on in situ measurements

Zhibo Zhang[1,2*], David B. Mechem[3], J. Christine Chiu[4], Justin A. Covert[3]

1. Physics Department, University of Maryland Baltimore County (UMBC), 1000 Hilltop Circle, Baltimore, Maryland, U.S.A.
2. Goddard Earth Sciences Technology and Research (GESTAR) II, UMBC, 5523 Research Park Drive, Baltimore, Maryland, U.S.A.
3. Department of Geography & Atmospheric Science, University of Kansas, 1251 Wescoe Drive, Room 3020, Lawrence, Kansas, U.S.A.
4. Department of Atmospheric Science, Colorado State University, 1371 Campus Delivery, Fort Collins, Colorado, U.S.A.

* Corresponding author address: Zhibo Zhang, Physics Department Room 418, UMBC, 1000 Hilltop Circle, Baltimore, Maryland, U.S.A. (Email: zzbatmos@umbc.edu)

Abstract

Because of the coarse grid size of Earth system models (ESM), representing warm-rain processes in ESMs is a challenging task involving multiple sources of uncertainty. Previous studies evaluated warm-rain parameterizations mainly according to their performance in emulating collision-coalescence rates for local droplet populations over a short period of a few seconds. The representativeness of these local process rates comes into question when applied in ESMs for grid sizes on the order of 100 kilometers and time steps on the order of 20-30 minutes. We evaluate several widely used warm-rain parameterizations in ESM application scenarios. In the comparison of local and instantaneous autoconversion rates, the two parameterization schemes based on numerical fitting to stochastic collection equation (SCE) results perform best. However, because of Jessen's inequality, their performance deteriorates when grid-mean, instead of locally-resolved, cloud properties are used in their simulations. In contrast, the effect of Jessen's inequality partly cancels the overestimation problem of two semi-analytical schemes, leading to an improvement in the ESM-like comparison. In the assessment of uncertainty due to the large time step of ESMs, it is found that the rain-water tendency simulated by the SCE is roughly linear for time steps smaller than 10 minutes, but the nonlinearity effect becomes significant for larger time steps, leading to

Early Online Release: This preliminary version has been accepted for publication in *Journal of the Atmospheric Sciences*, may be fully cited, and has been assigned DOI 10.1175/JAS-D-23-0198.1. The final typeset copyedited article will replace the EOR at the above DOI when it is published.

errors up to a factor of 4 for a time step of 20 minutes. After considering all uncertainties, the grid-mean and time-averaged rain-water tendency based on the parameterization schemes are mostly within a factor of 4 of the local benchmark results simulated by SCE.

Accepted for publication in *Journal of the Atmospheric Sciences.* DOI 10.1175/JAS-D-23-0198.1.

1. Introduction

"Warm rain" refers to the precipitation generated by the coalescence of water droplets without any ice-phase processes (Pruppacher and Klett 1998). Warm rain is prevalent in marine boundary layer (MBL) clouds (L'Ecuyer et a. 2009; Mülmenstädt et al. 2015; Zhang et al. 2022) that cover about a quarter of the ocean surface area (Wood 2012). Because of their strong radiative effects, MBL clouds play an important role in the global radiative energy budget (Klein and Hartmann 1993). MBL clouds interact with aerosols from both natural and anthropogenic sources leading to a number of cloud-mediated indirect effects such as changes to cloud radiative properties, precipitation production, and potentially, cloud lifetime (Twomey 1977; Albrecht 1989; Fan et al. 2016). For example, it is believed that an increase of aerosol loading can lead to smaller droplets and a weakened precipitation efficiency, which in turn could lead to a longer lifetime and stronger radiative cooling of MBL clouds (Albrecht 1989). In this second indirect or "cloud lifetime" effect, warm-rain processes play a key role in determining the influence of aerosol on cloud behavior (Wood et al. 2005a,b).

At present, our capability of simulating MBL clouds and their interaction with aerosols in global earth system models (ESM) is still limited. One important reason for this difficulty is that many of the physical processes in MBL clouds occur at spatial scales much smaller than the typical grid size of the current generation of ESMs (~100 km). As a result, these processes must be parameterized. Take the warm rain process for example. The initialization and growth of raindrops associated with the collision-coalescence processes can be reasonably simulated using so-called bin-microphysics (see review by Khain et al. 2015) or super-droplet methods (Shima et al. 2009). Unfortunately, these advanced methods cannot be adopted in the ESMs due to computational cost constraints. Instead, ESMs often adopt the "bulk" microphysics schemes that usually separate the whole droplet population into cloud and rain modes, each characterized by the so-called moments of the droplet size distribution (DSD). For example, many bulk microphysics schemes focused on the 0th and 3rd moments of the DSD corresponding to the number concertation and mass of the DSD, respectively. Some may include higher moments such as the 6th moment that corresponds to

Accepted for publication in *Journal of the Atmospheric Sciences.* DOI 10.1175/JAS-D-23-0198.1.

the radar reflectivity (Igel 2019). Interactions among these various partial moments of the drop-size distribution are then represented by a series of process-rate equations (Khain et al. 2015). For example, the birth of embryo raindrops through the coalescence of cloud drops is parameterized as an autoconversion process, and the growth of raindrops via collection of cloud droplets is parameterized as an accretion process. Many autoconversion and accretion parameterization schemes have been developed for use in ESMs, some based on theoretical analysis and derivations and others are based on numerical fitting of bin-microphysics results. A few widely used warm rain parameterization schemes are introduced in Section 2.

Because of the direct connection to the precipitation efficiency and thereby lifetime and radiative effects of MBL clouds, the autoconversion and accretion parameterizations are found to play a key role in determining the aerosol indirect effects in the ESMs (Jing et al. 2019; Mülmenstädt et al. 2020). Thus, it is critical to assess the accuracy and understand the limitations of commonly used warm rain parameterization schemes. An assessment was performed in Wood (2005), using DSDs from in situ measurements to drive a numerical stochastic collection equation (SCE) solver to diagnose the autoconversion and accretion rates. The diagnosed process rates were then used to assess the accuracy of several bulk warm rain parameterization schemes. It was found that the parameterized accretion rates agree well with those diagnosed from the SCE based simulations, but the autoconversion rates from some parameterizations disagree substantially. Using a similar approach, Hsieh et al. (2009) compared eight warm rain parameterizations with the SCE-based simulations driven by the measurements from two in situ airborne campaigns. They also found that bulk parameterizations, especially autoconversion schemes, are subject to substantial uncertainties in comparison to SCE-based results. It was found that the uncertainty associated with the assumed drop-size distribution can be a source of errors for process rates. For example, Gamma distributions fitted to the in situ measured DSDs can lead to substantial error in the computation of autoconversion rate due to poor fitting of the DSDs near the drop-drizzle separation size, even though the assumption provides a good approximation for the total coalescence rate computation.

Although Wood (2005) and Hsieh et al. (2009) provide a direct and rigorous assessment of bulk parameterization schemes, their evaluations were not carried out in the context of ESM applications and their focus is only on the local, instantaneous coalescence rates. In an ESM or

Accepted for publication in *Journal of the Atmospheric Sciences.* DOI 10.1175/JAS-D-23-0198.1.

numerical weather prediction model, on the other hand, the bulk autoconversion and accretion schemes must work with other components of the model, for example, sedimentation and evaporation processes, to achieve faithful simulations. For this reason, other studies have explored the behavior of bulk microphysics schemes and the implications for their performance in ESM simulations. For example, Suzuki et al. (2015) evaluated the warm rain simulations in several ESMs based on different bulk parameterization schemes by comparing the model simulated precipitation frequency and vertical profiles of radar reflectivity with satellite observations from MODIS (Moderate Resolution Imaging Spectroradiometer) and CloudSat. The evaluation revealed a common problem in the ESMs, specifically that they tend to produce light rain at a faster rate than that observed by satellite observations. This problem, often termed as "excessive drizzle", has also been noted in several other studies (Stephens et al. 2010, Wang et al. 2012; Song et al 2018a; Mülmenstädt et al 2020; Zhang et al. 2022). A similar satellite-based evaluation study by Song et al. (2018a) found that the MBL and warm rain simulations in one version of the Community Atmosphere Model (CAM) suffer from two major problems. The first is the excessive drizzle problem mentioned above. The second issue is that the model tends to produce a significant fraction of its MBL clouds that are too thin, in fact for satellite instruments to detect (i.e., "empty cloud"). They further found that the two problems are connected, and both caused by the unrealistically large "enhancement factor," a term to be explained below, in the subgrid warm rain parameterization.

Cloud microphysical properties such as cloud water content (q_c) and cloud droplet number concentration (N_c) can have significant variations at the scales smaller than the grid size of typical ESM. As pointed out in many previous studies, if the subgrid variations of cloud properties are not accounted for in the computation of grid-mean microphysical process rates, the result can be significantly biased as a consequence of Jensen's inequality (e.g., Pincus and Klein 2002; Larson and Griffin 2013; Weber and Quaas 2013; Boutle et al., 2014; Lebsock et al., 2013; Zhang et al 2019, 2021; Covert et al. 2022). This bias can be conceptually explained by a simple equation $f(\langle x\rangle) \neq \langle f(x)\rangle$ where $f(x)$ is any given parameterization scheme of warm rain and x the cloud property such as q_c and N_c. Ideally, the warm rain rate should be computed "locally" first to account for the subgrid variation of x and then averaged to obtain the grid mean value $\langle f(x)\rangle$. However, due to the lack of information on subgrid cloud variations, ESMs can only estimate the grid mean

Accepted for publication in *Journal of the Atmospheric Sciences.* DOI 10.1175/JAS-D-23-0198.1.

warm-rain process rates using the grid mean $<x>$ to compute $f(<x>)$. Because $f(x)$ for some components of warm-rain parameterizations is highly nonlinear, $f(<x>)$ is not equal to $< f(x)>$. Some ESMs try to account for this bias by introducing an enhancement factor E, such that $E \cdot f(<x>)$ is closer to the desired $< f(x)>$. This simple correction, however, can also cause problems as shown in Song et al. (2018).

On the one hand, studies like Suzuki et al. (2015) and Song et al. (2018a) have a larger scope than Wood (2005) and Hsieh et al. (2009) as they try to develop a comprehensive understanding of the performance of warm rain parameterizations in the host ESMs including the coupling of warm rain with other model components. On the other hand, their evaluations are inevitably affected by many issues other than warm rain parameterizations which makes it difficult to pinpoint the cause of the model-observation differences. For example, Song et al. (2018b) elucidated that the uncertainty associated with the COSP (Cloud Feedback Model Intercomparison Project Observation Simulator Package) radar simulator can contribute to the substantial difference between MBL cloud radar reflectivity simulated by CAM-COSP and observations from CloudSat, which in turn can be misinterpreted as the excessive drizzle problem.

The main objective of this study is to better understand the uncertainties associated with the warm rain parameterization schemes as used in ESMs with two new perspectives. First, in addition to evaluation of local rate $f(x)$ through comparison with the SCE-simulated results (e.g., Wood (2005); Hsieh et al. (2009)), we will evaluate the grid mean estimation $f(<x>)$ to gain a comprehensive understanding of the performance of the parameterization scheme in the context of ESM applications. This will be achieved without invoking a host ESM, and thereby we avoid the interacting influences of the other components of ESM that complicate sources of errors as shown in Suzuki et al. (2015) and Song et al. (2018a). Second, we will investigate the sensitivity of simulations to the time-step size used in the warm rain parameterization schemes in ESMs. Most warm rain parameterization schemes are developed to capture the instantaneous rate and thus evaluated against instantaneous SCE calculations (e.g., Wood 2005; Khairoutdinov and Kogan (2000); Chiu et al. 2021). However, the typical time step used in ESM is on the order of 20–30 minutes, even though cloud microphysical properties leading to drizzle onset might evolve substantially faster. While sub-stepping is possible at the cost of increased computation time, the

Accepted for publication in *Journal of the Atmospheric Sciences*. DOI 10.1175/JAS-D-23-0198.1.

warm rain rates are always assumed to be invariant within any integration time-step in ESMs. The error associated with this assumption of constant process rates will be quantified to better inform the modeling strategy.

We will use the SCE-based simulations as the benchmark for evaluation, which are driven by in-situ measurements from a recent airborne field campaign detailed in section 2. A brief overview of the bulk parameterization schemes to be evaluated will be also provided. In section 3, a comprehensive analysis of the three sources of uncertainty as mentioned above will be presented. The results will be summarized and discussed in Section 4.

2. Data and Methodology

2.1. In situ measurements from the ACE-ENA campaign

The observations used for this study are from the Aerosol and Cloud Experiments in Eastern North Atlantic (ACE-ENA) airborne measurements campaign (Wang et al., 2022). During the two intensive observation periods (IOPs) of the campaign, one in summer of 2017 and the other in winter of 2018, the Gulfstream-1 aircraft of the Atmospheric Radiation Measurement (ARM) program funded by the Department of Energy (DOE) was deployed for over 30 research flights (RFs) around the ARM ENA site to sample a large variety of cloud and aerosol properties along with the meteorological conditions. The data collected from the ACE-ENA campaign have been used in many recent studies of aerosol, cloud, and their interactions (see a recent review by Wang et al. 2022). In our own recent study, the droplet size distribution (DSD) measurements from the Fast Cloud Droplet Probe (FCDP) and Two-Dimensional Stereo (2D-S) Probe were used to investigate the vertical dependence of the horizontal variability of cloud microphysical properties (Zhang et al. 2021; Covert et al. 2022). The same set of data and the same method to select the RFs are used in this study, which will be briefly summarized below.

To drive the SCE-based simulations of the droplet collision-coalescence process, we use the merged DSD product based on the combination of FCDP, 2-DS and High Volume Precipitation Spectrometer (HVPS) instruments that together cover the diameter range from 1.5 μm to 9075 μm

Accepted for publication in *Journal of the Atmospheric Sciences.* DOI 10.1175/JAS-D-23-0198.1.

(Mei and Ermold 2023). The product is available at a frequency of 1 Hz. Since the typical horizontal speed of the G-1 aircraft during the in-cloud leg is about 100 m s^{-1}, the spatial resolution of this product is on the order of 100 m. Following the same criteria and procedures described in Zhang et al. (2021), we selected a total of seven RF cases, three from summer 2017 IOP and 4 from the winter 2018 IOP. These selected RFs have multiple continuous in-cloud samples at different vertical levels with the horizontal flight legs of at least 10 km and cloud fraction larger than 10%. Here a 1 Hz segment of the flight track is defined as cloudy if the measured q_c is larger than a threshold value (i.e., $q_c > 0.01$ g kg^{-3}). In addition, the chosen cases must have at least one vertical penetration leg to be used to identify the vertical extent and microphysical structure (i.e., q_c and N_c) of the cloud (see more details in Section 3 of Zhang et al. 2021). Figure 1 shows an example of the selected RF observed on July 18, 2017. A common sampling pattern of the ACE-ENA campaign is to repeat the horizontal level runs multiple times in a "L" shape. Figure 1a shows examples of these legs, which are flown at different vertical levels inside, above, and below the cloud and are referred to as "hleg" in this paper. The two sides of the L-shape hleg are usually perpendicular and parallel to the wind direction, respectively. Using the method described in Zhang et al. (2021), a total of 7 hlegs inside of the MBL cloud are identified from the July 18, 2017 RF and used for this study (see yellow-shaped regions in Fig 1a). Among them, helg #8 and #12 are close to the top of the MBL cloud, according to collocated ground-based radar observations. The duration of these selected hlegs is between 580 and 700 s, with their total horizontal length is roughly 60 km and each side of the L-shape being about 30 km. Following the same process as the July 18, 2017 RF case, we identified and selected a total of 32 hlegs from the 7 selected RF cases. More characteristics of these selected hlegs can be found in Zhang et al. (2021).

As mentioned above, one of the objectives of this study is to understand the effects of subgrid cloud heterogeneity on the performance of warm rain parameterization schemes. The selected hlegs are used in this study as analogues of ESM grids. For example, helg #12 in Fig. 1a can be considered as a virtual ESM grid with a size of about 30 km. The merged DSD measurement for hleg #12 is shown in Fig. 1b. Clearly, there is a significant horizontal variation in the DSDs. There are about 580 DSD observations for this hleg, each with a spatial resolution of ~100 m. In this study, we shall refer to them as the "local" or "subgrid" observations. From these local observations, we can derive the local rate *f(x)* (e.g., autoconversion or accretion rates) and then

Accepted for publication in *Journal of the Atmospheric Sciences.* DOI 10.1175/JAS-D-23-0198.1.

average the local rate over the flight leg to obtain grid-mean rate <*f(x)*>. Alternatively, we can first average the local observations to grid mean <*x*> and then calculate the process rate *f*(<*x*>) using the grid-mean properties. The difference between two sets of computations will help us understand the effects of subgrid heterogeneity on warm rain parameterization schemes as applied to the virtual ESM grids represented by the selected hlegs.

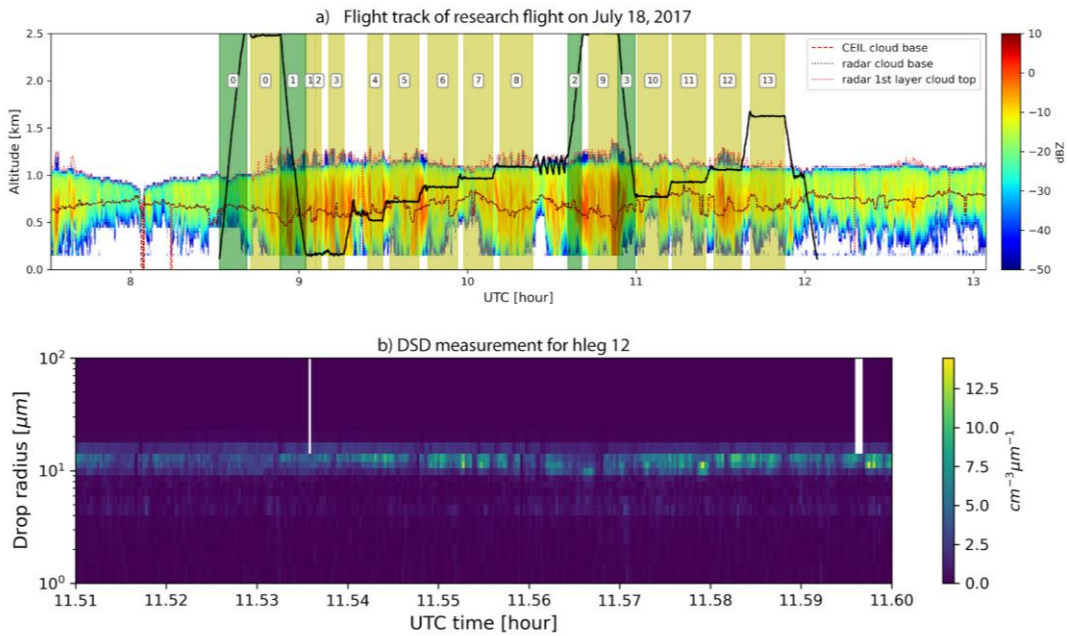

Figure 1 a) The vertical flight track of Gulfstream-1 aircraft (thick black line) overlaid on the radar reflectivity contour by the ground-based KZAR (Ka-band ARM zenith cloud radar). The dotted lines in the figure indicate the cloud base and top retrievals from ground-based radar and ceilometer instruments. The yellow-shaded regions are the "hlegs". B) The DSD measurement from the merged FCDP, 2DS and HVPS product for the hleg #12 close to cloud top.

It should be noted that the In situ measurements used in this study are inherently one-dimensional (1-D) data sampled alone the flight tracks. It is known that such sampling schemes can lead to statistical errors and biases when compared to two-dimensional (2D) data (Stephens et al. 2010). However, it is difficult, if not impossible, to overcome this sampling limitation using

Accepted for publication in *Journal of the Atmospheric Sciences*. DOI 10.1175/JAS-D-23-0198.1.

in situ observations alone. In future studies we will investigate this error using, for example, large-eddy-simulations (Covert et al. 2022).

2.2. Diagnosis of benchmark process rates based on stochastic collection equation (SCE)

In this study, the benchmark used to evaluate the warm rain parameterizations is the SCE-based simulations driven by size-resolved DSDs. As explained in Wood (2005a), most warm rain parameterization schemes separate the whole droplet population into two modes, a cloud mode with $r<r^*$ and a rain mode with $r>r^*$, where r^* is the critical radius for the separation. We set r^* as 25 μm in this study, a size commonly employed as a lower bound for drizzle drops (Khairoutdinov and Kogan 2000; Wood 2005a; Wood et al. 2011; Glienke et al. 2017). After the size separation, the coalescence of droplets can also be separated into two processes, the autoconversion (referred to as "AU" for short) where the coalescence of cloud-mode droplets forms raindrops, and the accretion (referred to as "AC" for short) where the coalescence of raindrops with cloud droplets form larger raindrops. Given a size-resolved DSD, the autoconversion and accretion rates can be simulated accurately using numerical SCE solvers. In this study we use the numerical SCE solver developed by Bott (1998) for the calculator which has been successfully verified against both analytical solutions and the Berry–Reinhardt scheme (Bott 1998).

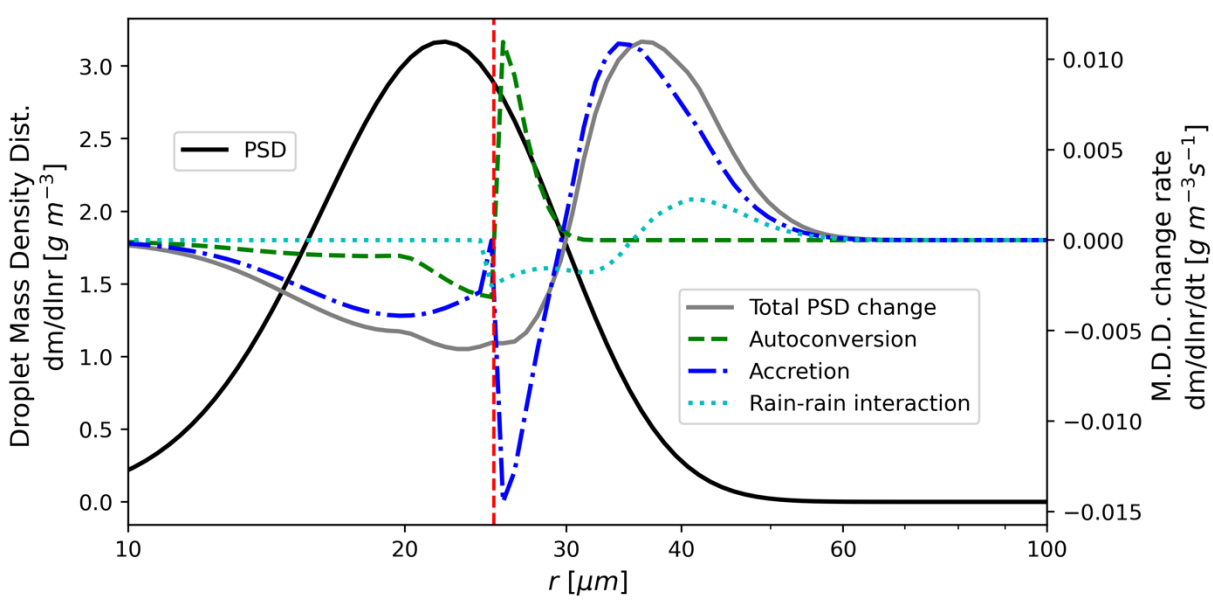

Accepted for publication in *Journal of the Atmospheric Sciences*. DOI 10.1175/JAS-D-23-0198.1.

Figure 2 An example to demonstrate the diagnosis of autoconversion and accretion rates using Bott (1998) numerical SCE solver and a hypothetical Gamma DSD (solid black line). The total change of droplet mass distribution simulated by the SCE (solid gray line) is the result of autoconversion (dashed green line), accretion (dash-dotted blue line) and interactions between two raindrops (dotted canyon line). The vertical red line represents the threshold r^* to separate cloud and rain modes.

Figure 2 shows an example based on assumed Gamma DSD to demonstrate the diagnosis of autoconversion and accretion rates using the Bott (1998) numerical SCE solver. Given a DSD (solid black line), expressed here as a droplet mass density distribution, the SCE solver integrated over one second yields a reduction of droplet mass between 10 µm and 30 µm and an increase of mass between 30 and 50 µm (solid gray line). This evolution of the DSD is attributed to three processes: autoconversion (dashed green line), accretion (dash-dotted blue line), and interactions between two raindrops (dotted cyan line). To diagnose the rain water tendency due to autoconversion, a special run of the SCE solver is performed where only interactions between cloud droplets with $r<r^*$ is allowed. The accretion rate is diagnosed by running the SCE solver to simulate only interactions between cloud droplet and raindrop. Finally, the coalescence of two raindrops (so-called "self-collection") can also lead to a DSD change, but it does not generate new rain water and so is not considered here.

It should be noted that the evolution of DSD due to coalescence, and therefore autoconversion and accretion, are time dependent. In the example in Figure 2, the time step is only one second. As explained in the Introduction, the typical time step of ESMs is 20–30 minutes. Ideally, the computations should be performed at a number of intervals, e.g., every second, and then integrated to obtain an accurate estimate of the autoconversion and accretion rates. But it is too time consuming, and most ESMs simply assume that the rates are constant during the time step of 20–30 minutes. In this section 3, we will investigate the uncertainty caused by this assumption.

2.3. Warm rain parameterization schemes

We evaluate four autoconversion parameterizations, each of which can be classified into one of the two groups. The first group includes the widely used scheme developed by Khairoutdinov and

Accepted for publication in *Journal of the Atmospheric Sciences.* DOI 10.1175/JAS-D-23-0198.1.

Kogan (2000) ("KK2000 scheme" hereafter) and a new scheme developed by Chiu et al. (2021) ("Chiu2021 scheme" hereafter). These two schemes were developed through numerical fitting of autoconversion and accretion rates, based on SCE calculations either as implemented into a large-eddy simulation model (KK2000) or driven by DSDs from in situ measurements (Chiu et al. 2001). A common function for such fitting is a power law form. The second group includes the schemes developed by Liu et al. (2007) ("Liu2007 scheme" hereafter) and Seifert and Beheng (2001) ("SB2001 scheme" hereafter). They attempt to construct analytical and physically insightful expressions for the parameterization. To achieve this, they first simplify the SCE by replacing the complicated collision-coalescence kernel with a simple analytical approximation. Then, they apply the simplified SCE to a mathematically convenient DSD such as the Gamma DSD to derive analytical expressions for the autoconversion and accretion rates. The SB2001 and Liu2007 schemes are therefore referred to as "semi-analytical" schemes in this study.

For accretion, we only consider two sets of parameterization schemes, KK2000 and Chiu2021. We consider only two because previous studies have shown that warm rain parameterization schemes differ mainly in terms of autoconversion, whereas the accretion schemes are similar and all agree reasonably well with the bin microphysics results (e.g., Wood 2005b). In addition, the KK2000 and Chiu2021 accretion schemes are simple to implement, yielding a reduced computational cost. The details of these schemes are provided below.

2.3.1. KK2000 and modified KK schemes

The KK2000 scheme parameterizes the autoconversion rate using a power function of cloud water content (CWC) q_c and cloud droplet number concentration (CDNC) N_c as

$$\left(\frac{\partial q_r}{\partial t}\right)_{AU} = 1350 q_c^{2.47} N_c^{-1.79}, \tag{1}$$

where $\left(\frac{\partial q_r}{\partial t}\right)_{AU}$ is the autoconversion rate in terms of changes in rain water mass mixing ratio (q_r; kg kg^{-1}) per time (t; s^{-1}), and q_c and N_c have units of kg kg^{-1} and cm^{-3}, respectively. The parameter 1350 and the two exponents 2.47 and −1.79 are obtained through a nonlinear regression between

Accepted for publication in *Journal of the Atmospheric Sciences.* DOI 10.1175/JAS-D-23-0198.1.

the variables q_c and N_c and the autoconversion rate derived from large-eddy simulation (LES) with bin-microphysics spectra. Similarly, the accretion rate $\left(\frac{\partial q_r}{\partial t}\right)_{AC}$ is parameterized as:

$$\left(\frac{\partial q_r}{\partial t}\right)_{AC} = 67(q_c q_r)^{1.15}. \tag{2}$$

Perhaps because of its simplicity and reasonable performance, the KK2000 autoconversion and accretion expressions in Eq. (1) and (2) have been adopted by many ESMs, such as the CAM (Morrison and Gettleman 2008) and Energy Exascale Earth System Model (E3SM) (Rasch et al. 2019), although various modifications and tunable parameters have been introduced in the model development process. One thing interesting to note is that the KK2000 was originally developed for the use in high-resolution LES not ESMs.

Because all the parameters used in the KK2000 schemes are obtained from numerical regression, they are arguably *not* constrained by any physical rules and therefore their values can be tuned to change the results to desired direction. For example, Gettelman et al. (2013) argued that the ratio of accretion to autoconversion rate based on the original KK2000 scheme is too small and should increase with the total cloud water path based on the comparisons with in-situ observations from a field campaign. Furthermore, they believed that the differences in the accretion-to-autoconversion ratio between parameterization and observations were largely attributable to autoconversion, which motivated the change of the parameterization in Eq. (1) to the following (Gettleman et al. 2021):

$$\left(\frac{\partial q_r}{\partial t}\right)_{AU} = 13.50 q_c^{2.47} N_c^{-1.1}, \tag{3}$$

where the new autoconversion rate exponent on N_c (−1.1) and prefactor (13.5) have been adjusted from the original Eq. (1) to tune the auto-conversion rate to the observation-based estimation reported in Gettleman et al. (2019). In this study, we shall refer to it as the "modified KK2000" scheme.

Accepted for publication in *Journal of the Atmospheric Sciences.* DOI 10.1175/JAS-D-23-0198.1.

2.3.2. Chiu2021 scheme

In Chiu et al. (2021), autoconversion and accretion parameterization schemes are developed using a machine-learning (ML) algorithm that is trained based on SCE-based calculations. Although the ML-based schemes are most accurate when compared to the benchmark results, they do not have an explicit, closed-form mathematical expression and therefore are arguably not directly comparable to other schemes in this study. In addition to the ML-based scheme, Chiu et al. (2021) also developed an autoconversion scheme using the "conventional" power-law function as follows

$$\left(\frac{\partial q_r}{\partial t}\right)_{AU} = 16.8 q_c^{2.015} N_c^{-0.746} N_r^{0.640}, \tag{4}$$

where all variables are in the International System (SI) units. In comparison with SCE-based simulations, the scheme in Eq. (4) has a relative uncertainty between −39% and 55% and a mean bias around 8% (Chiu et al. 2021). What is interesting about Eq. (4) is that the parameterized autoconversion rate depends on not only the cloud mode properties (q_c and N_c) but also rain mode property N_r even though by definition the autoconversion is a result of coalescence of two cloud mode drops. It was argued that the dependence of autoconversion scheme on N_r represents the influence from the evolution stage of the cloud DSD, which is related to the first appearance of nascent raindrops. Interested readers are referred to the section 5 of Chiu et al (2021) for in-depth discussion. Similar to Eq. (4), a "conventional" accretion rate was also constructed in Chiu et al. (2021) as follows

$$\left(\frac{\partial q_r}{\partial t}\right)_{AC} = 69.5 q_c^{1.148} q_r^{1.159}, \tag{5}$$

also in SI units. The accretion scheme in Eq. (5) has a relative uncertainty between −23% and 21% and a mean bias around −6%. In this study, we will refer to the parameterization schemes in Eq. (4) and (5) and the "Chiu2021" scheme. Finally, a noteworthy detail about Chiu et al. (2021) is that their SCE-based simulations used the in-situ measurements of DSDs from the ACE-ENA campaign as inputs. Although the case selection standards and data processing procedures may be different, the benchmark results used in Chiu et al. (2021) and this study are overall similar and consistent.

Accepted for publication in *Journal of the Atmospheric Sciences.* DOI 10.1175/JAS-D-23-0198.1.

2.3.3. SB2001 scheme

Taking a different approach from KK2000 and Chiu2021, the SB2001 scheme is developed based on physical insights into the collision-coalescence processes and mathematical derivations instead of numerical fitting. After a number of assumptions and simplifications, the following analytical formula was derived for the autoconversion rate,

$$\left(\frac{\partial q_r}{\partial t}\right)_{AU} = \frac{k_c}{20x^*}\frac{(\mu+2)(\mu+4)}{(\mu+1)^2}q_c^3 N_c^{-1}\left[1+\frac{\Phi_{au}(\tau)}{(1-\tau)^2}\right], \tag{6}$$

where $k_c = 9.44 \times 10^{-9}$ cm^3 g^{-2} s^{-1} and $x^* = 2.6 \times 10^{-7}$g are two constants. The term $\left[1+\frac{\Phi_{au}(\tau)}{(1-\tau)^2}\right]$ is an adjustment factor that accounts for the dependence of autoconversion rate on the temporal evolution of the DSD. In this term, $\tau = 1 - q_c/(q_c + q_r)$ is a dimensionless parameter being zero for $q_r = 0$ corresponding to the very beginning of the coalescence growth and one for $q_c = 0$ corresponding to a situation when all cloud droplets have been converted to raindrops. The function $\Phi_{au}(\tau)$ can be parameterized as $\Phi_{au}(\tau) = 600\tau^{0.68}(1-\tau^{0.68})^3$.

It should be noted that the derivation of Eq. (6) was enabled by several assumptions. An Important one is that the shape of the cloud mode DSD follows the Gamma distribution $n_c(r) = Ar^{\mu}e^{-\Lambda r}$, where μ is the so-called spectra shape parameter and Λ is a scale parameter. This assumption leads to the $(\mu+2)(\mu+4)$ / $(\mu+1)^2$ term in Eq. (6) to account for the dependence of the autoconversion rate on the shape of Gamma DSD, which gives the host ESM that uses Eq. (6) an extra degree of freedom to control and tune the warm rain parameterization (Liu et al. 2007). Although the assumption of a Gamma DSD is necessary for the derivation of Eq. (6) and widely used in ESMs, it poses a challenge for the comparison with observation-based results, because the observed DSDs used to drive SCE simulation are often poorly or insufficiently described using a Gamma distribution. Ideally, a Gamma DSD must be fitted from the observed DSD first and then the corresponding q_c, N_c and μ used in Eq. (6). However, as pointed out in previous studies, this step of DSD fitting is highly uncertain and can lead to large errors (Hsieh et al. 2009), which is

Accepted for publication in *Journal of the Atmospheric Sciences*. DOI 10.1175/JAS-D-23-0198.1.

confirmed by our own fitting analysis (not shown). Moreover, the results based on the fitted DSDs are not comparable to the results based on KK2000 and Chiu2021 schemes. Based on these considerations, we avoid the DSD fitting in this study and use the q_c and N_c directly derived from the observed DSD in Eq. (6). As such, q_c and N_c, which have dominant roles in Eq. (6), are closely linked to observations. For the value of μ, we adopt the parameterization scheme used in Morrison and Gettelman (2008) $\mu = 1/\eta^2 - 1$, where η is the relative radius dispersion of the size distribution. It is in turn assumed to be a function of N_c (in unit of cm^{-3}) as $\eta = 0.000571N_c + 0.2714$. Although the parameterization of μ introduces uncertainty, we consider this inevitable when applying Eq. (6) to realistic DSDs.

2.3.4. Liu2007 scheme

Sharing a similar motivation and philosophy to SB2001, the Liu2007 scheme was developed based on physical insights into the collision-coalescence processes and advanced mathematical derivations and simplifications. The derivation process is too tedious and complex to explain in detail here, but the final autoconversion rate in the Liu2007 scheme is given as follows:

$$\left(\frac{\partial q_r}{\partial t}\right)_{AU} = \left(\frac{3}{4\pi\rho_w}\right)^2 \kappa_2 \left(x_c^2 + 2x_c + 2\right)(1 + x_c)e^{-2x_c} N_c^{-1} q_c^3, \tag{7}$$

where ρ_w is the density of water, contant $\kappa_2 = 1.9 \times 10^{11}$ cm^{-3} s^{-1}, and $x_c = 9.7 \times 10^{-17} N_c^{3/2} q_c^{-2}$ is the ratio of the critical to mean masses. Note that x_c here is only a numerical approximation to its full form in Liu et al. (2005) and only valid numerically when N_c is in the unit of cm^{-3} and q_c in the unit of $g\ cm^{-3}$.Readers who are interested in the derivation process and the underlying physics of Eq. (7) are referred to Liu et al. (2004, 2005, 2006a,b, 2007) for details. Similar to SB2001, the derivation of the Liu2007 scheme is based on several assumptions and simplifications. An important one is that the DSD follows the general Weibull distribution $n_c(r) = \frac{\zeta N_c}{r_0^\zeta} r^{\zeta-1} exp\left[-\left(\frac{r}{r_0}\right)^\zeta\right]$, where ζ is a constant related to the relative dispersion of the DSD. Furthermore, the derivation of Eq. (7) assumes a value of ζ=3. Similar to the shape parameter μ in the SB2001 scheme, the value of ζ can be tuned or parameterized in the host ESM. However, the Liu2007 parameterization faces the same challenges as the SB2001 scheme when being applied

Accepted for publication in *Journal of the Atmospheric Sciences*. DOI 10.1175/JAS-D-23-0198.1.

to direct observations of DSDs, where realistic DSDs often deviate from the assumed DSD (in this case, the Weibull distribution). To avoid the uncertainties caused by numerical fitting of DSD, we directly use the Eq. (7) for the Liu2007 scheme in this study.

3. Warm rain parameterization uncertainty analysis

3.1. Uncertainty in parameterization of local instantaneous rates

As explained in the Introduction, we are interested in the performance of the above warm rain parameterization schemes at different spatial (local vs. grid mean) and temporal scales (instantaneous vs. time-step average). To this end, we first examine the local instantaneous results. As an example, Figure 3a shows q_c and N_c for hleg #12, which was sampled near cloud top at ~1 km as shown in Figure 1a. Values of q_c and N_c were computed by integrating the merged DSD product described in Section 2.1 from the smallest bin to the separation threshold r^*=25 μm. Apparently, both q_c and N_c exhibit significant variations. While the mean values of q_c are around a few tenths of g m^{-3}, episodic low values are seen throughout the hleg with smallest value being about 0.01 g m^{-3}. These features are probably cloud holes associated with the evaporation of cloud water after mixing with the entrained air from cloud top (Gerber et al. 2005). A similar feature is also seen in the plot of N_c with its mean value around 70 cm^{-3} and episodic low values down to 20 cm^{-3}. Interestingly, the low values of q_c and N_c are almost perfectly aligned, which leads to a high correlation coefficient over 0.9. The high correlation between q_c and N_c suggests that the cloud top entrainment in this case is mostly inhomogeneous where the reduction of q_c is caused by the complete evaporation of some cloud droplets at all sizes rather than a shift in droplet DSD toward smaller sizes with CDNC unchanged.

The implications of the high correlation between q_c and N_c for the simulation of autoconversion has been discussed in depth Zhang et al. (2019; 2021). In short, the horizontal variations of q_c and N_c usually lead an enhancement in the parameterization of grid mean autoconversion rate. The total enhancement can be accounted by a factor EF, a product of E_q, E_N, and E_{COV} that represents the enhancement due to variability of q_c and N_c, and their coverability, respectively. For an

Accepted for publication in *Journal of the Atmospheric Sciences*. DOI 10.1175/JAS-D-23-0198.1.

idealized case of a bivariate lognormal distribution, the positive correlation between q_c and N_c leads to a term E_{COV} that is smaller than unity and counteracts the effects of E_q and E_N.

Figure 3b shows the rain water content q_r and raindrop number concentration N_r for drops with radius $r>r^*$, which are orders of magnitude smaller than q_c and N_c as expected. The strong radar reflectivity (dBZ ~0) below the hleg #12 in Figure 1a suggests the presence of significant precipitation in the lower part of the cloud and below cloud, which is initialized by the coalescence process at cloud top. A close examination of Figure 3a and Figure 3b reveals a positive correlation between q_c and q_r. Lebsock et al. (2013) also noticed a positive correlation between the q_c and q_r retrieved from MODIS and CloudSat for marine low-level clouds with a global mean correlation coefficient of 0.44. Similar to the correlation between q_c and N_c, the correlation between q_c and q_r can have an impact on the parameterization of grid-mean accretion rate through its role in the enhancement factor (Lebsock et al. 2013).

Accepted for publication in *Journal of the Atmospheric Sciences.* DOI 10.1175/JAS-D-23-0198.1.

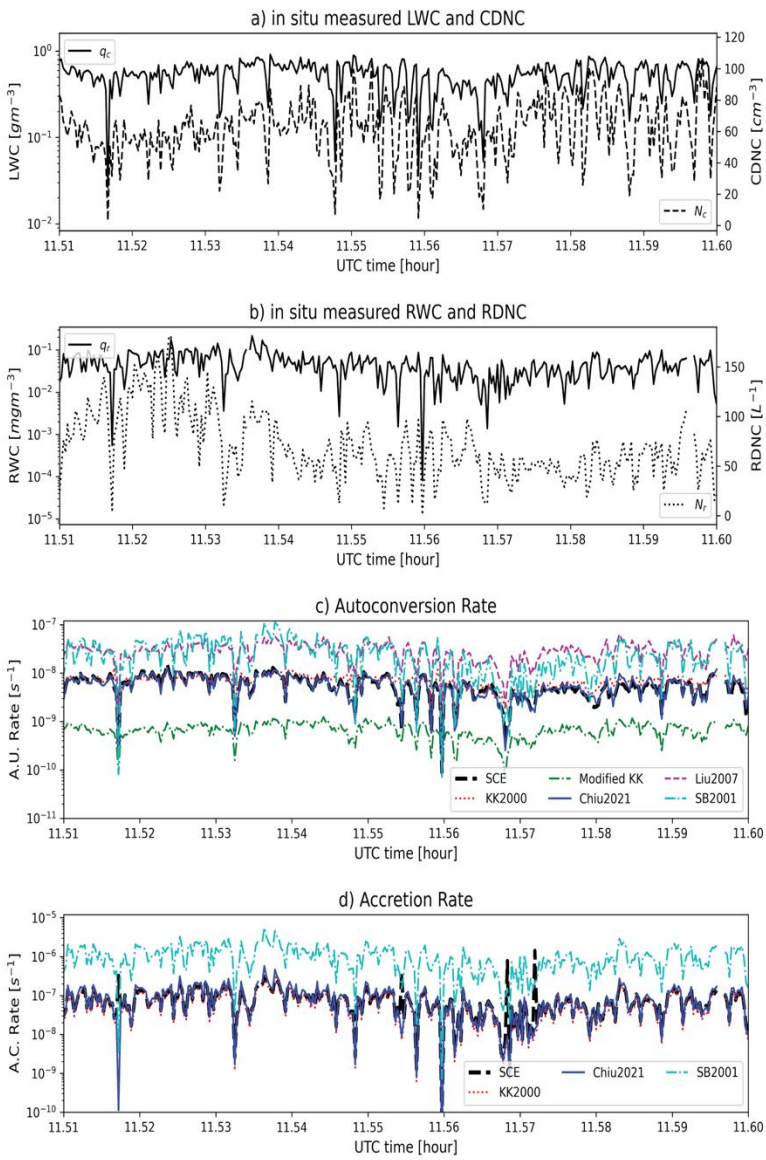

Figure 3 In-situ measured (a) cloud water content (CWC; q_c), cloud droplet number concentration (CDNC; N_c), and (b) rain water content (RWC; q_r) and rain drop number concentration (RDNC, N_r) for hleg #12 of RF on July 18, 2017 shown in Figure 1. The corresponds (c) autoconversion and (d) accretion rates based on the SCE simulations and various parameterization schemes.

Substituting the q_c, N_c, q_r and N_r from the observations into the parameterization schemes described in Section 2, we derived autoconversion rates shown in Figure 3c and accretion rates in Figure 3d for hleg #12. For comparison purposes, we also used the observed DSD in Figure 1b to

Accepted for publication in *Journal of the Atmospheric Sciences*. DOI 10.1175/JAS-D-23-0198.1.

drive the SCE-based simulations to derive the benchmark values. In the SCE simulation, we used a time step of one second. A sensitivity study of using a range of time steps from a few tenths of second to a few seconds leads to only negligible differences (<5%). Among the five tested schemes, SB2001 and Liu2007 significantly overestimate autoconversion while the modified KK2000 scheme underestimates the benchmark autoconversion rate from the SCE simulation. In comparison, the two schemes based on numerical fitting, KK2000 and Chiu2021, agree with the benchmark results very well. When averaged over the whole hleg, KK2000 (mean value 6.63 $\times 10^{-9}$ s^{-1}) overestimates the SCE result (mean value 5.35 $\times 10^{-9}$ s^{-1}) by only 20% and the Chiu2021 (mean value 5.35 $\times 10^{-9}$ s^{-1}) is even within 2%. The good performance of Chiu2021 is expected because as aforementioned it was developed based on the same set of data as this study. The substantial error associated with the SB2001 and Liu2007 parameterizations is probably because they are developed based on the assumption of certain shapes of DSD (see Section 2 for discussion) but the measured discrete DSDs are more complex and deviate from their assumptions.

Figure 3d shows the comparison of local and instantaneous accretion rates between the SCE-based simulation and two parameterization schemes, KK2000 and Chiu2021. Evidently, both schemes are in excellent agreement with the benchmark results. This is not surprising because as one can see from Eq. (2) and (5) the two schemes are very similar, and several previous studies have found that the accretion rate based on KK2000 scheme is an excellent approximation to the SCE-based simulation (Wood 2005 and Chiu et al. 2021)

Accepted for publication in *Journal of the Atmospheric Sciences.* DOI 10.1175/JAS-D-23-0198.1.

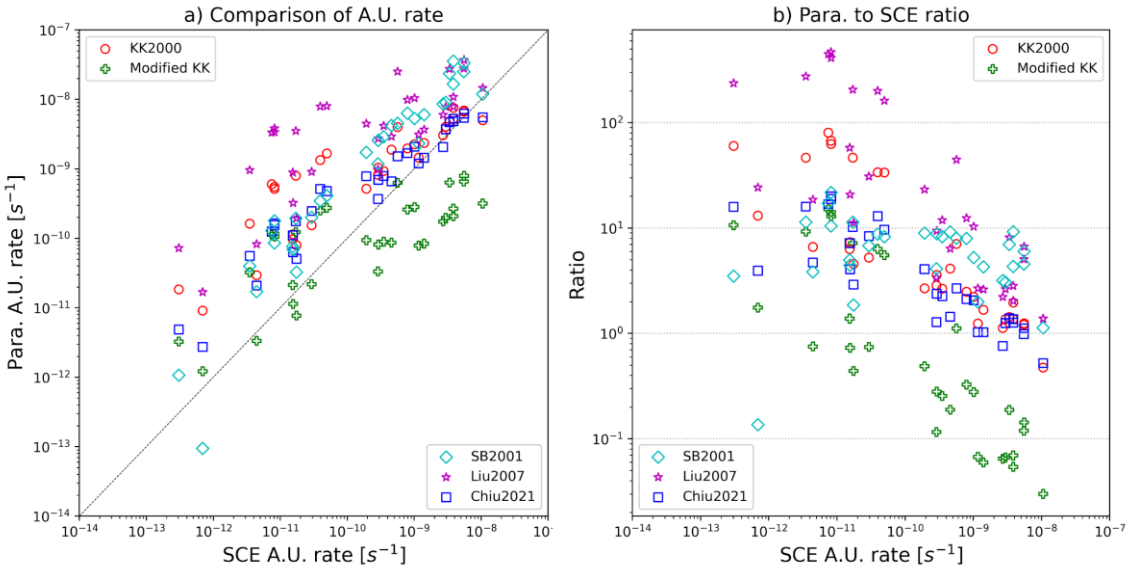

Figure 4. a) A comparison of the autoconversion rate between SCE simulations and bulk parameterizations schemes for all 32 selected hlegs, and b) the ratio of parameterization to SCE simulations as a function of SCE benchmark of autoconversion rate. Note that in both SCE simulations and bulk parameterization the rate is computed first locally and then averaged over each hleg, so that the subgrid variability of cloud properties are accounted for.

As explained in the Introduction, the objective of this study is to assess the warm rain parameterization schemes in the context of ESM applications. The selected horizontal in situ flight legs of sufficient length, such as hleg #12, are intended to emulate a grid of ESM. Therefore, after deriving the local instantaneous autoconversion and accretion rates for every observation point, we average the results over the hleg to obtain the hleg-mean results. We consider these results an analogue of the grid-mean results of an ESM grid and refer to them as the "grid-mean" results. We carried out the same computation and averaging process as hleg 12 for all the 32 selected hlegs. Figure 4a shows a comparison of the grid-mean autoconversion rate between the SCE-based calculations and different parameterization schemes, each point in the figure representing a selected hleg. Interestingly, the points appear to cluster into two large groups, one with the benchmark grid-mean autoconversion rate from SCE simulation smaller and the other larger than 10^{-10} s^{-1}. In the first group, the modified KK2000 scheme agrees better with the benchmark results than other schemes that all tend to overestimate the benchmark. As shown in Figure 4b, the

Accepted for publication in *Journal of the Atmospheric Sciences*. DOI 10.1175/JAS-D-23-0198.1.

Liu2007 and KK2000 scheme can overestimate the benchmark results by as much as two orders of magnitude (~50–500), while the SB2001 and Chiu2021 scheme perform slightly better with the ratios to the benchmark values mostly around 10. In the second group with the benchmark grid-mean autoconversion rate larger than 10^{-10} s^{-1}, the KK2000 and Chiu2021 agree best with the benchmark results. Clearly, the modified KK2000 and SB2001 scheme tend to underestimate and overestimate the benchmark results, respectively. The Liu2007 scheme has a similar accuracy as KK2000 and Chiu2021 for the few cases with the largest grid-mean autoconversion rates but overall tend to overestimate. When considering the two groups together, the newest Chiu2021 scheme apparently has the best overall accuracy, followed by the KK2000 and SB2001 schemes.

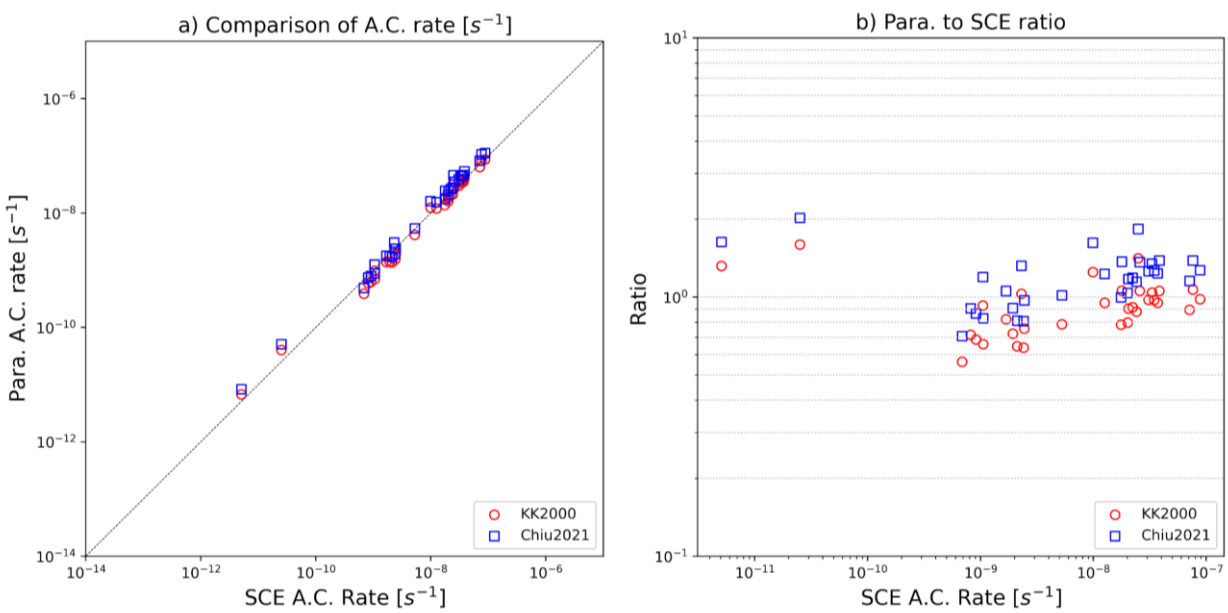

Figure 5 Same as Figure 4 except for accretion rate simulation.

Now we turn to the comparison of accretion rate. As shown in Figure 5, KK2000 and Chiu2021 have almost identical accretion rates, which is not surprising given the similarity between Eqs. (2) and (5). Same as previous studies (e.g., Wood 2005b), we found both of them to agree with the SCE-simulations very well, within a factor of 2, which is impressive considering the fact that the accretion rates themselves vary over several orders of magnitude.

Accepted for publication in *Journal of the Atmospheric Sciences*. DOI 10.1175/JAS-D-23-0198.1.

3.2. Uncertainty due to subgrid variability

The grid-mean autoconversion rates in Figure 4 are aggregated from the local rates at the subgrid scale. Such aggregation is impossible in ESMs due to the lack of subgrid information. Instead, the ESMs can only estimate the autoconversion and accretion rates based on the grid-mean properties, i.e., $<q_c>$, $<N_c>$, $<q_r>$, $<N_r>$, yielding process rates that are not equal to the true grid-mean results because of Jessen's inequality. This difference is illustrated in Figure 6 based on the hleg 14 from the RF on July 20th, 2017. Figure 6a shows the joint histogram between the N_c and q_c for this hleg on logarithmic scales, with the dashed lines indicating the grid-mean values of $<q_c>$ and $<N_c>$. As a result of the subgrid variability, the subgrid autoconversion rates span several orders of magnitude from 10^{-15} s^{-1} to 10^{-9} s^{-1} with the mean value (vertical solid line) between 10^{-11} s^{-1} to 10^{-10} s^{-1} (see histogram in Figure 6b). The orange histogram in Figure 6b shows the subgrid variability of autoconversion rates simulated based on the KK2000 scheme as an example. The vertical dashed line indicates the grid-mean autoconversion rate based on the integration of the aggregation of subgrid values. In comparison, the vertical dotted line represents the grid-mean autoconversion rate computed using the KK2000 scheme and the grid-mean $<q_c>$ and $<N_c>$. In other words, the difference between the vertical dashed line and dotted line is a result of the Jessen's inequality, and the difference between the vertical dotted line and solid line is the difference between what would be simulated in an ESM using the KK2000 scheme and the "true" grid mean autoconversion rate that is simulated based on the SCE and aggregated from the local (i.e., subgrid) values.

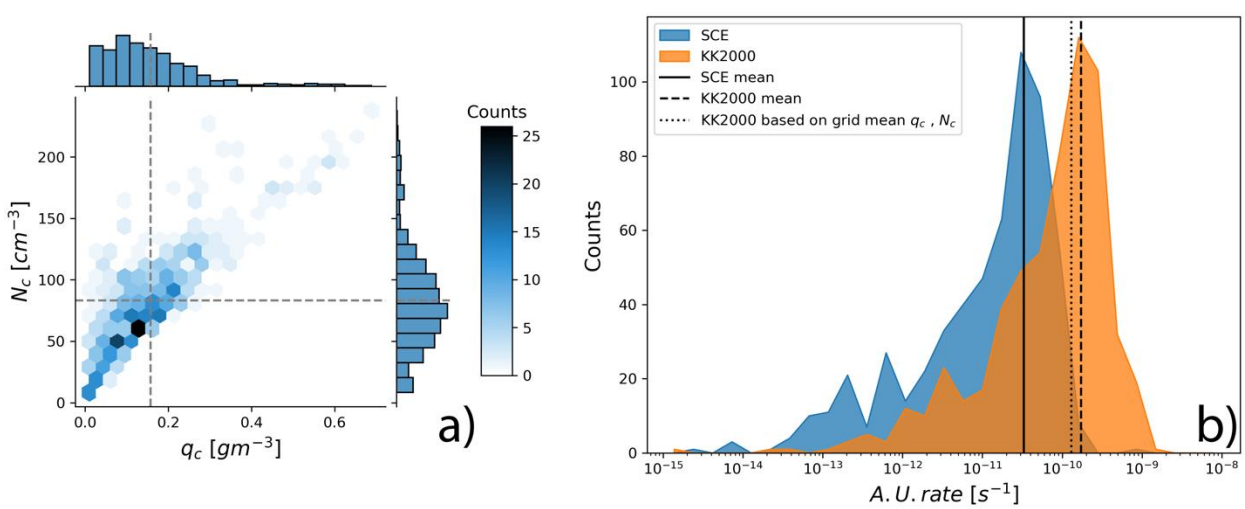

Accepted for publication in *Journal of the Atmospheric Sciences*. DOI 10.1175/JAS-D-23-0198.1.

Figure 6 a) The joint and marginal PDFs of N_c and q_c for hleg 14 from the RF on July 20th, 2017. b) The PDF of the AU rate based on SCE-simulations and KK2000 parameterizations. Different vertical lines correspond to different methods to estimate the grid-mean AU rate. See text for detail.

Following previous studies (Pincus and Klein 2002, Larson and Griffin 2013, Zhang et al. 2019, 2021), we define an enhancement factor as follows to quantify the impact of Jessen's inequality on the computation of grid-mean autoconversion rate

$$EF = \frac{\frac{1}{N}\sum_{i=1}^{N} f\left(q_{c,i}, N_{c,i}, q_{r,i}, N_{r,i}\right)}{f(< q_c >, < N_c >, < q_r >, < N_r >)}, \tag{8}$$

where the function $f()$ represents a given warm rain parameterization scheme described in Section 2. The numerator represents the grid-mean rate aggregated from the subgrid values, where $f()$ first operates on the local properties $q_{c,i}, N_{c,i}, q_{r,i}, N_{r,i}$ with the subscript i indicating each observation point and then local process rates are averaged to obtain grid-mean value (e.g., the vertical solid line in Figure 5b). Note that not all the autoconversion schemes need all of these four variables; we merely include them all to indicate that a scheme might depend on any combination of them. The denominator represents the ESM type computation of grid-mean rates, where the function $f()$ operates on the grid-mean properties, $< q_c >, < N_c >, < q_r >, < N_r >$ (e.g., the vertical dotted line in Figure 6b). The magnitude of EF depends on two main factors, the nonlinearity of the parameterization scheme $f()$ and the subgrid heterogeneity of $q_{c,i}, N_{c,i}, q_{r,i}, N_{r,i}$. In general, given the same ESM grid and associated subgrid heterogeneity, the more nonlinear the parameterization function $f()$ is, the stronger the impact of Jessen's inequality and therefore the larger the EF is. Similarly, given a parameterization function $f()$, an ESM grid with larger subgrid heterogeneity usually has a larger EF (Zhang et al. 2019, 2021). Among several different indices to quantify the subgrid heterogeneity, the relative dispersion is one of the most frequently used, which is defined as the ratio between the standard deviation of a variable and its mean value. For example, the relative dispersion of subgrid water content is $\eta = std(q_c)/< q_c >$.

Accepted for publication in *Journal of the Atmospheric Sciences.* DOI 10.1175/JAS-D-23-0198.1.

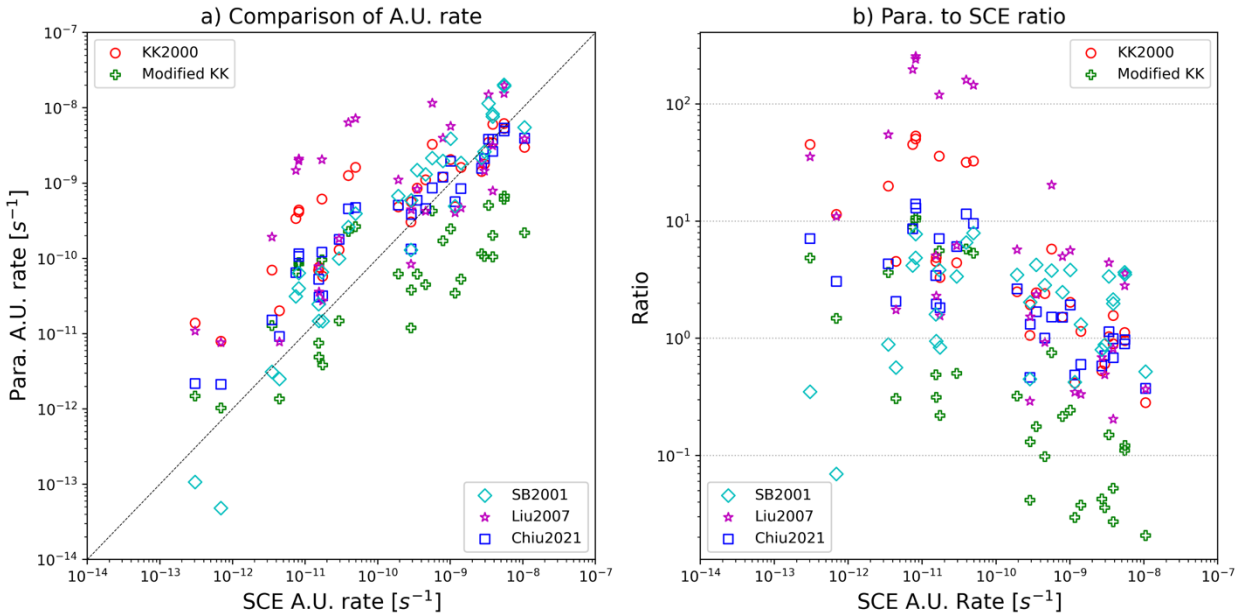

Figure 7. Same as Figure 4 except that we replace the parameterized grid-mean rate with that simulated based on the grid-mean properties (i.e., the denominator in Eq. (8)) and therefore the parameterized autoconversion rate include both parameterization uncertainty and effects by Jessen's inequity.

Figure 7a shows the EFs derived based Eq. (8) for the 32 selected hlegs as a function of the relative dispersion of subgrid cloud water content. Clearly, among the five autoconversion parameterization schemes, the Liu2007 is most affected by Jessens's equality followed by SB2001, with their EFs up to 10. In other words, the autoconversion rate estimated based on the grid mean properties, $f(< q_c >, < N_c >, < q_r >, < N_r >)$ can be an order of magnitude smaller than the "true" grid mean value. In contrast, the EFs of the three numerical schemes, KK2000, modified KK2000 and Chiu2021, are significantly smaller, mostly lower than 3. This difference is probably caused by two factors. First, the SB2001 and Liu2007 are apparently more nonlinear. The exponent of q_c is 3 in both schemes, in comparison to 2.47 in the KK2000 scheme and 2.015 in the Chiu2021. Second, both schemes have extra highly nonlinear terms, in addition to the power law of q_c and N_c, such as the three terms involving x_c in Eq (7) for the Liu2007 scheme and the adjustment factor term involving τ in Eq. (6).

Accepted for publication in *Journal of the Atmospheric Sciences*. DOI 10.1175/JAS-D-23-0198.1.

After understanding the impact of Jessen's inequality on each parameterization, we now investigate how it affects the comparison between the "true" grid-mean values (calculated by averaging the local process rates over each flight leg) and estimates of the grid-mean rates calculated using leg-mean values of q_c, N_c, etc. The latter is taken to represent ESM-simulated grid-mean rates where the true subgrid variability is unknown. Recall that in Figure 4b, we compared the "true" grid-mean autoconversion rate, which is simulated based on the SCE and aggregated from subgrid values, and the parameterized grid-mean rate simulated based on the parameterization function and aggregated from subgrid values (i.e., the numerator in Eq.(8)). In other words, the effect of Jessen's inequality was not included in the comparison. In Figure 7b, we updated the comparison by replacing the parameterized grid-mean rate with that rate based on the grid-mean properties (i.e., the denominator in Eq. (8)). As such, the parameterized values now include two sources of errors, the parameterization error (Figure 4) and the effect of Jessen's inequality (Figure 7a). In comparison with Figure 4b, the ratios of the parameterized to the "true" grid-mean rates shift systematically to smaller values. This is consistent with the fact that the EFs are mostly larger than unity. Among the five schemes, the KK2000 and Chiu2021 schemes are only slightly affected as indicated by small EF values. Although the EF for the modified KK2000 scheme is comparable to that of Chiu2021, its overall performance is further deteriorated because the effect of Jessen's inequality makes the scheme that is already biased low even more biased. On the contrary, for the SB2001 and Liu2007 schemes the effect of Jessen's inequality tends to partly cancel out their overestimation problem, leading to an overall improvement of their performance in terms of estimating the "true" grid-mean autoconversion rates.

Several points can be made based on the above observations of Figure 7. First, most warm rain parameterization schemes are developed to provide a good fit to the local rates. When they are applied in an ESM setting to obtain grid-mean process rates, Jessen's inequality can lead to systematic underestimation bias which can either help improve through error cancellation or even worsen the overall performance of the parameterization scheme. Second, some ESMs try to use an EF to account for the effect of Jessen's inequality (Morrison and Gettelman 2008). As pointed out by Zhang et al. (2019, 2021), such attempts face several limitations, such as the ignorance of subgrid CDNC variation in their estimation of the EF. In addition, the results in Figure 7 question whether the effectiveness of an EF approach to fulfill its purpose. For example, for the modified

Accepted for publication in *Journal of the Atmospheric Sciences.* DOI 10.1175/JAS-D-23-0198.1.

KK2000 scheme the introduction of EF can help improve the grid-mean simulate results because it helps partially cancel the underestimation bias caused by the parameterization scheme itself and Jessen's inequality. On the contrary, for Liu2007 and SB2001 the introduction of EF can nullify the marginal improvement of these schemes as a result of a favorable error cancellation between the parameterization scheme itself and the Jessen's inequality. These findings cast doubt on the ability of a single EF to improve grid-mean microphysical process rates for the correct reason. On the other hand, it can be used as a tuning parameter to account for systematic bias associated with the microphysical parameterizations and as a result of subgrid variability (Rotstayn et al. 2000; Jing et al. 2017, Mülmenstädt et al., 2020, 2021).

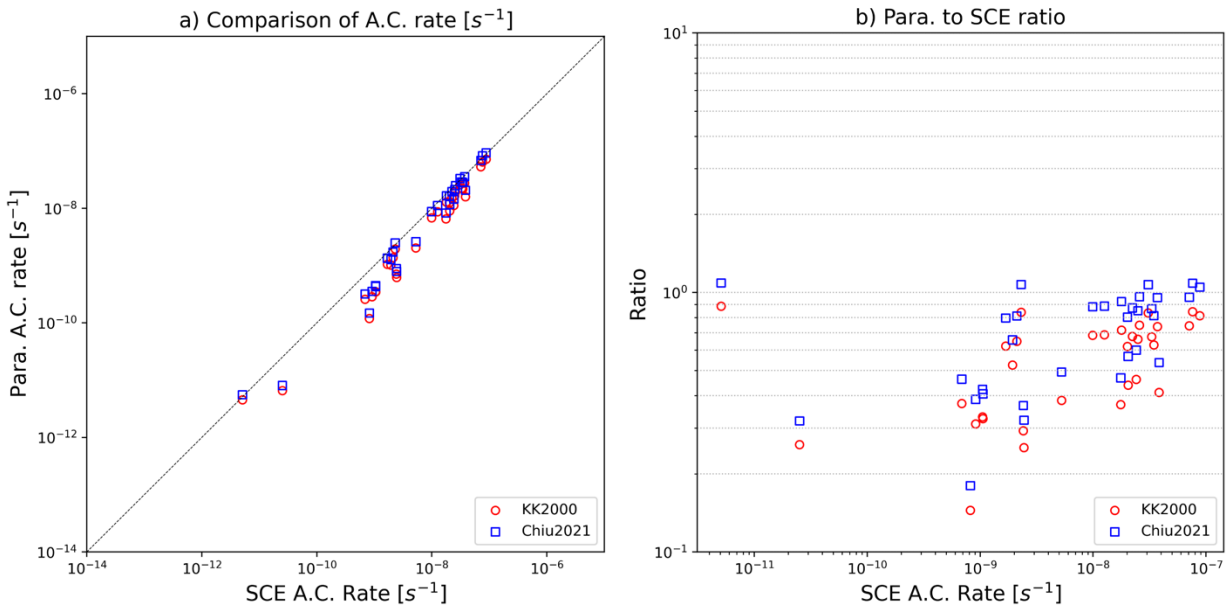

Figure 8. Same as Figure 5 except that we replace the parameterized grid-mean rate with that simulated based on the grid-mean properties (i.e., the denominator in Eq. (8)) and therefore the parameterized accretion rate includes both parameterization uncertainty and effects by Jessen's inequity.

The impacts of subgrid cloud variation on accretion rate simulation is shown in Figure 8. A couple of observations can be made. First, the effect of Jessen's inequality leads to a systematic underestimation of accretion rate by both schemes (Fig. 8a), with KK2000 slightly more affected. Different from the impact on autoconversion rate simulation, where the parameterization uncertainty is dominant (Figure 4b vs. Figure 7b), Jessen's inequality caused by subgrid variations

Accepted for publication in *Journal of the Atmospheric Sciences*. DOI 10.1175/JAS-D-23-0198.1.

has a more significant and systematic impact on the representation of accretion (Figure 5b vs. Figure 8b) because parameterization uncertainty is relatively small. Second, the effect of Jessen's inequality on the accretion rate is comparable to that on autoconversion in Figure 7a for the KK2000 and Chiu2021 schemes, mostly smaller than 2. This is interesting because autoconversion schemes are usually more nonlinear than accretion schemes (e.g., Eq. (1) vs. Eq (2)) in terms of the q_c dependence and therefore many previous studies expect it to be more prone to Jessen's inequality. This is a misconception because they only considered the effect of subgrid of q_c on the enhancement factor but overlooked the subgrid variation of N_c. As elucidated by Zhang et. al. (2019, 2021) the usual positive correlation between q_c and N_c tends to compensate for the effects caused by subgrid variations of q_c and N_c, leading to a smaller-than-expected enhancement factor for autoconversion parameterizations.

3.3. Uncertainty in time integration

In the last section, we examined the impacts of subgrid cloud property variations on the computation of grid-mean rates for different parameterization schemes. In this section, we visit the uncertainty associated with the time integration. Many warm rain parameterization schemes, such as KK2000, are developed for LES but are nevertheless applied in ESM applications. The long time steps of ESMs ~10–30 minutes, compared to a few seconds for LES, can cause several potential issues for parameterization schemes (e.g., Yu and Pritchard 2015; Gettelman and Morrison 2015). For example, in a prognostic precipitation scheme that aims to simulate precipitation processes explicitly, the sedimentation process is especially sensitive to the length of time step, which has significant implications for aerosol indirect and cloud radiative effects (Gettelman and Morrison 2015). In the context of warm rain simulations, an ESM assumes constant autoconversion and accretion rates that are diagnosed based on the initial condition for the whole time step even though the shape of DSD and thereby collision coalescence processes change significantly over the timestep. This uncertainty is illustrated using a hypothetical example in Figure 9. Here we used a DSD following the Gamma distribution with an effective radius of 15 μm and CDNC of 100 cm^{-3} to drive the SCE simulation with a high-frequency time step of dt = 1 s. Figure 9a and b show the time evolution of mass and number concentration of the DSD a from t = 0 s to t = 1200 s. As expected, the autoconversion process leads to the rise of the rain mode

Accepted for publication in *Journal of the Atmospheric Sciences.* DOI 10.1175/JAS-D-23-0198.1.

drops which become more and more pronounced as time increases. An ESM with a large time step dt_{ESM} faces two uncertainties when simulating such DSD evolutions. First, the ESM only evaluates the rain water tendency based on the initial conditions, i.e., $\left[\left(\frac{\partial q_r}{\partial t}\right)_{AU} + \left(\frac{\partial q_r}{\partial t}\right)_{AC}\right]\Big|_{t=0}$ and then use it to estimate the rain water generated during the whole time step, i.e., $\Delta q_r = q_r(t = dt_{ESM}) - q_r(t = 0) = \left[\left(\frac{\partial q_r}{\partial t}\right)_{AU} + \left(\frac{\partial q_r}{\partial t}\right)_{AC}\right]\Big|_{t=0} \cdot dt_{ESM}$. As such, the total rain mass Δq_r is simply a linear function of time because of assuming constant rates that are diagnosed based on the initial condition, in contrast to the nonlinear time dependent rain mass simulated based on an evolving DSD. This difference can lead to −60% relative error for dt_{ESM} ~ 1200 s. We shall refer to this uncertainty as the "nonlinearity of rain water tendency". The second uncertainty in ESMs is caused by the bulk parameterization schemes. As shown in the previous sections, some schemes can be more accurate than others in terms of simulating instantaneous rates at the initial time. However, whether they are as accurate when being applied to larger time steps remains unknown and questionable. For example, thanks to error cancellation a bulk parameterization scheme that overestimates the instantaneous rates at the initial time could lead to better results than the other scheme that is highly accurate for an instantaneous calculation, when both applied dt_{ESM} ~ 1200 s simulation for the example in Figure 9.

Accepted for publication in *Journal of the Atmospheric Sciences.* DOI 10.1175/JAS-D-23-0198.1.

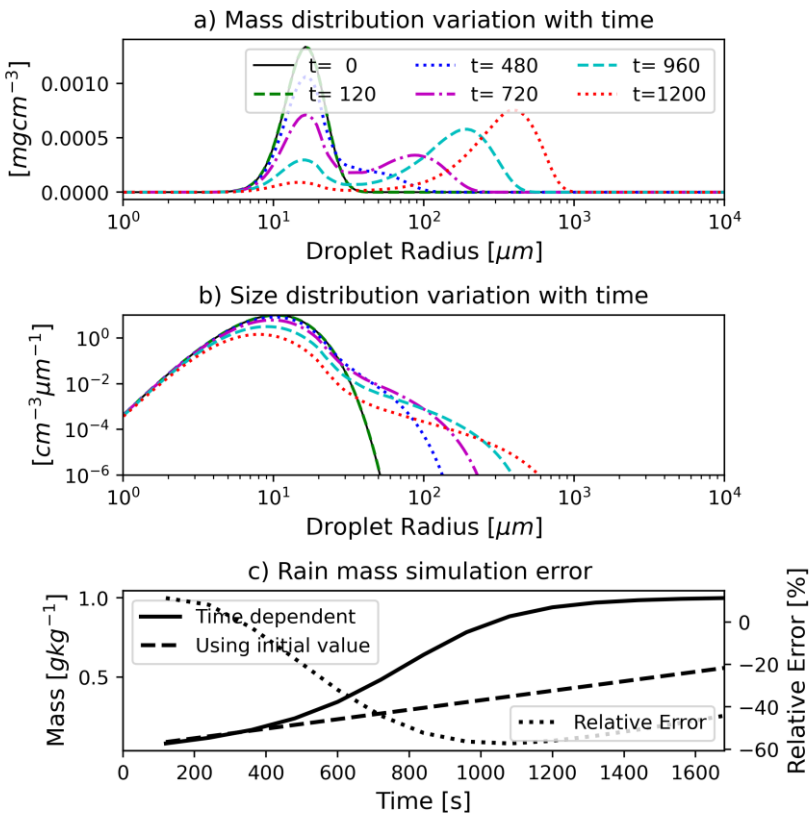

Figure 9. The temporal evaluation of a) mass and b) droplet size distribution of a hypothetical DSD following the Gamma distribution, and c) the corresponding error of the rain mass simulation diagnosed using the initial values in comparison with the time-dependent simulations.

We first examine the nonlinearity of rain water tendency in terms of temporal revolution in the context of ACE-ENA in situ measurements. We focus on the comparison of SCE-based simulations at different time steps to avoid the complication by parameterization uncertainties. Specifically, we run the SCE-based collision-coalescence simulations for each measured DSD in each selected hlegs continuously with a dt = 1s for 1200 s, allowing the DSDs to evolve over time. From these simulations, we derive the time-averaged rain water tendency for each selected hleg for typical ESM time steps, i.e., 300 s, 600 s, 900 s, and 1200s, as follows

Accepted for publication in *Journal of the Atmospheric Sciences*. DOI 10.1175/JAS-D-23-0198.1.

$$\langle\overline{\left(\frac{\partial q_r}{\partial t}\right)_{dt_{ESM}}}\rangle = \frac{<q_r(dt_{ESM})>-<q_r(t=0)>}{dt_{ESM}},\ dt_{ESM}\text{=1s, 300s, 600s, 900s, 1200s} \tag{9}$$

where $< q_r(dt_{ESM}) >$ is the rainwater content at dt_{ESM} from the SCE simulations averaged over the hleg, $< q_r(t = 0) >$ is the initial rain water content averaged over the hleg, $\langle\overline{\left(\frac{\partial q_r}{\partial t}\right)_{dt_{ESM}}}\rangle$is mean rain water tendency averaged over both time (dt_{ESM}) and space (hleg), with the overhead bar indicating temporal average and angle brackets the spatial average. Note that in the SCE computations of instantaneous rain water a small time step Δt =1 s is used. Evidently, if $< q_r(\Delta t) >$ is linear with respect to Δt then the rainwater tendency is a constant independent of time. As a result, the instantaneous rain water tendency diagnosed from the initial condition is accurate and can be used for longer time steps. However, if the $< q_r(\Delta t) >$ is highly nonlinear then the use of instantaneous value as the mean rainwater tendency can lead to significant error which is the focus of our investigation here. It should be noted that we have combined the autoconversion and accretion in Eq (9). Although a further decomposition is possible, it is hardly meaningful because once the shape of DSD evolves with time, the corresponding autoconversion and accretion rates are not comparable with their initial values. To avoid being overwhelmed by details, we focus on the combined results of autoconversion and accretion in the rainwater content.

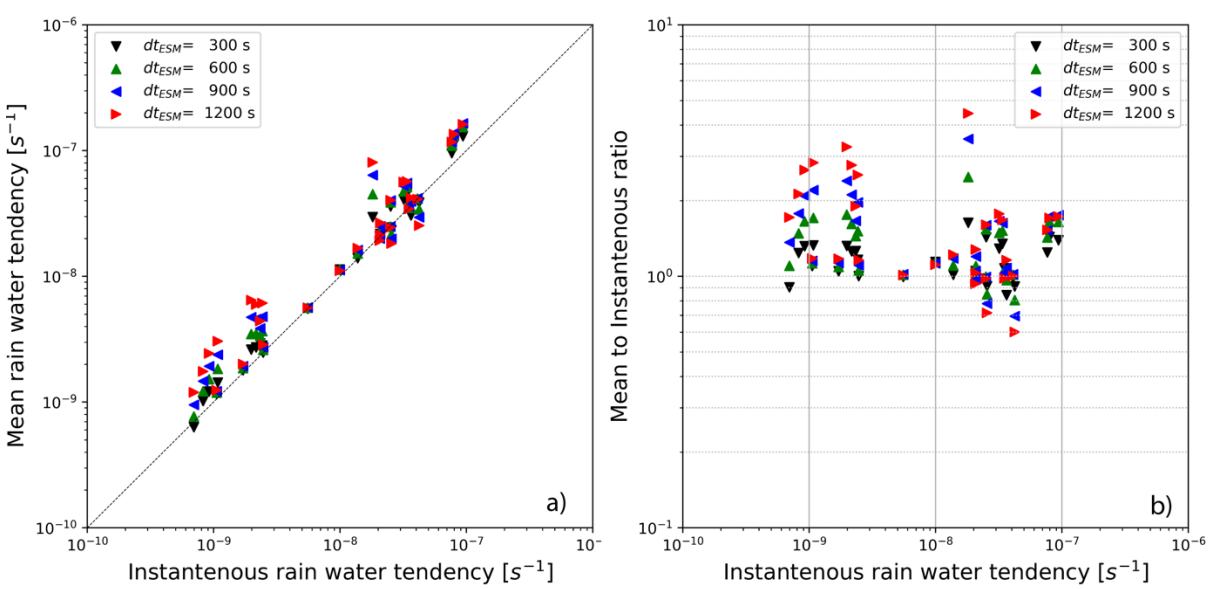

Accepted for publication in *Journal of the Atmospheric Sciences*. DOI 10.1175/JAS-D-23-0198.1.

Figure 10 a) A comparison between the mean rain water tendency averaged over various ESM time steps and instantaneous value diagnosed from the initial conditions. b) The ratio between the mean and instantaneous rain water tendency.

Figure 10 shows the comparison of instantaneous rain water tendency diagnosed based on the initial values with the time-averaged rain-water tendency for the selected hlegs calculated over four dt_{ESM} (300s, 600, 900, and 1200 s). As expected, for the smallest dt_{ESM} = 300 s the mean values are very close to the instantaneous values with a relative error within 50%, indicating that the DSD changes are small and the rain water tendency is approximately linear with time. However, as dt_{ESM} increases, the mean values gradually deviate from the instantaneous values. For the largest time step dt_{ESM}= 1200 s, the ratio of mean to instantaneous rain water tendency (Figure 10b) can vary from 0.6 up to a factor of 4. Among all 32 selected hlegs, 26 have the mean value larger than the instantaneous value. To better understand the cause for the difference, we selected an hleg from the RF on Jan. 26th, 2018 for further analysis, which has the highest ratio (a factor of 4.4) of mean to instantaneous rain water tendency for dt_{ESM} = 1200 s. Figure 11a shows the temporal evaluation of the domain averaged DSD of this hleg based on the SCE simulation from the initial condition to dt_{ESM} = 1200 s. Figure 11b shows the corresponding autoconversion and accretion rates diagnosed from the SCE simulation (see section 2.2). Apparently, for this hleg the rain water is mainly generated by the accretion process which is orders of magnitude larger than the autoconversion. As the DSD evolves, the accretion rate increases with time instead of being a constant, probably due to the rise of the rain mode mass around 300~400 μm. In contrast, the value of autoconversion rate remains largely constant within dt_{ESM}= 1200 s. As a result of increasing accretion rate, the rain water tendency diagnosed from the initial conditions underestimate the time-averaged value for this hleg. We found this to be a common pattern after examining a few other hlegs.

Accepted for publication in *Journal of the Atmospheric Sciences.* DOI 10.1175/JAS-D-23-0198.1.

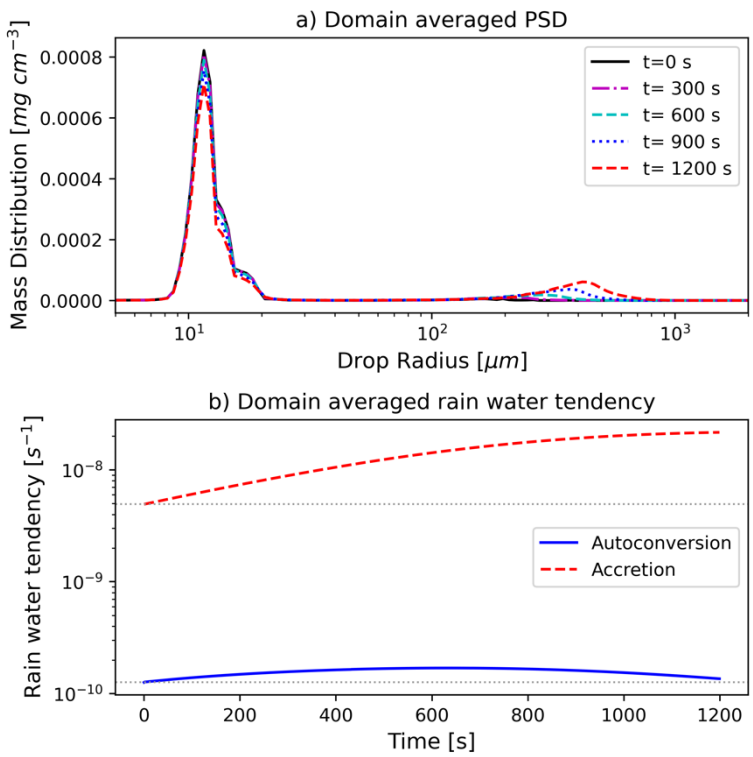

Figure 11 a) the temporal evolution of mean droplet mass distribution averaged over a hleg from the RF on Jan. 26th, 2018; and b) the corresponding autoconversion and accretion rates based on the SCE-simulation.

In the above analysis, the comparison is between SCE simulations at different time steps. Now we include the uncertainty associated with the parameterization in the analysis. Similar to the above analysis, the temporal (averaged over the dt_{ESM} time step) and spatial (averaged over the hleg) average of the rain water tendency are used as the benchmark for the analysis. For comparison, we compute the corresponding ESM-like rain water tendency as the sum of the autoconversion and accretion rates that are both diagnosed from the initial conditions at $t = 0$

$$\langle \overline{\left(\frac{\partial q_r}{\partial t}\right)_{dt_{ESM}}} \rangle_{ESM} = f_{AU}(< X(t=0) >) + f_{AC}(< X(t=0) >) \tag{10}$$

where f_{AU} and f_{AC} are the parameterization schemes for autoconversion and accretion, respectively; $< X(t=0) >$ indicates the initial cloud properties averaged over the hleg. As such,

Accepted for publication in *Journal of the Atmospheric Sciences*. DOI 10.1175/JAS-D-23-0198.1.

the ESM-like rain water tendency from Eq. (10) includes three major sources of variability: 1) the parameterization uncertainty associated with f_{AU} and f_{AC}, 2) the uncertainty caused by Jessen's inequality due to the use of spatially averaged cloud properties and 3) the uncertainty caused by approximating time-dependent tendency with a constant value that is diagnosed from the initial conditions. We include the SB2001 and Liu 2007 parameterizations in the comparison by combining their formulations for autoconversion f_{AU} with the Chiu2021 accretion parameterization in Eq. (5) for f_{AC}, as it performs very well in the previous comparison.

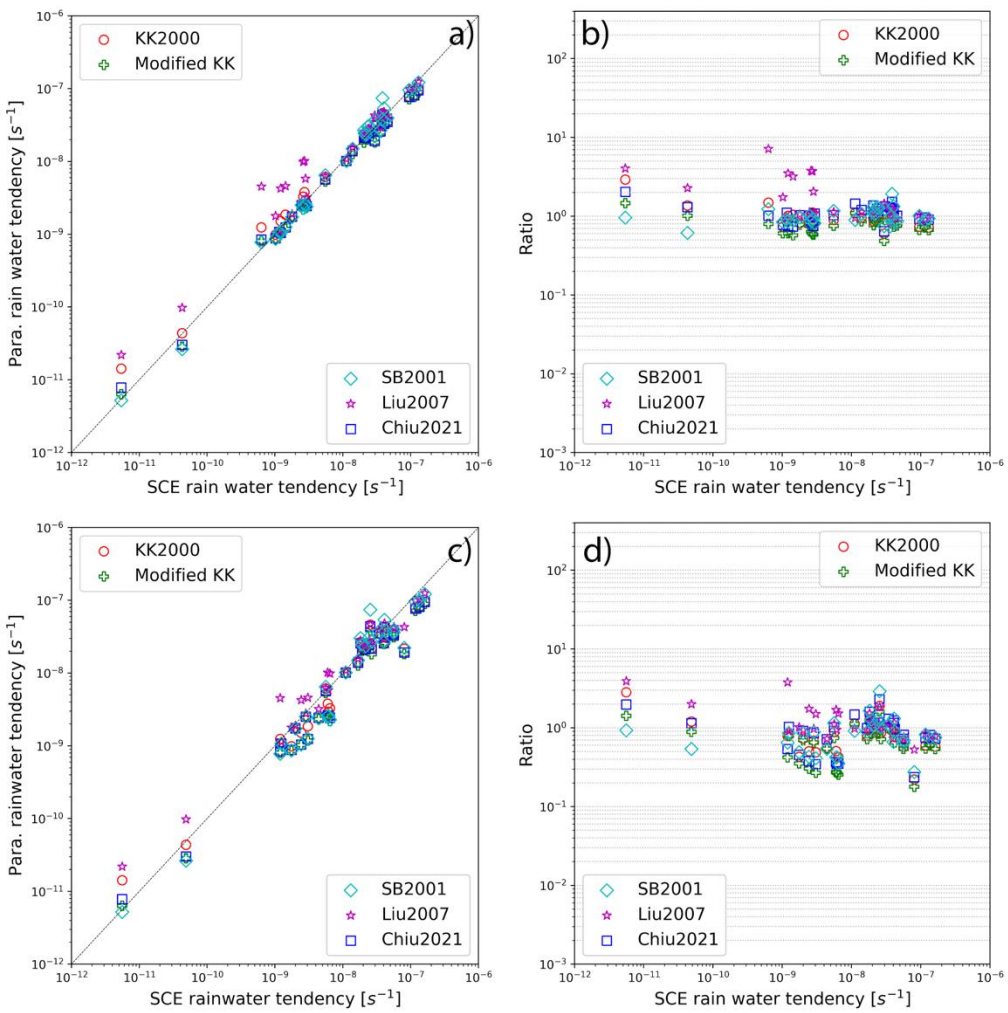

Accepted for publication in *Journal of the Atmospheric Sciences*. DOI 10.1175/JAS-D-23-0198.1.

Figure 12 A comparison of rain water tendency between ESM-like simulations based on Eq. (9) using different parameterization schemes and the benchmark results for two time steps, dt_{ESM} = 300 s (a and b) and dt_{ESM}=1200 s (c and d).

Figure 12 shows the comparison of rain water tendency between ESM-like simulations based on different parameterization schemes and the benchmark results for two time steps, dt_{ESM} = 300 s and dt_{ESM} = 1200 s. As shown in Figure 12a and b, for a small dt_{ESM}= 300 s, the ESM-like simulations agree with the benchmark results reasonably well, with the ratios between the two mostly between 0.4 and 4, except for the simulation based on Liu2007 scheme which tends to overestimate the benchmark, up to a factor of 6. Considering the comparison results in Figure 4 and 6, this overestimation of Liu2007 is caused by the autoconversion bias. Note that from dt_{ESM} = 300 s to dt_{ESM} = 1200 s, the rain water tendencies from ESM-like simulations remain constant, only the SCE-simulated benchmark results change. As analyzed above, for most hlegs the time averaged rain water dependency for dt_{ESM} = 1200 s is larger than that for dt_{ESM} = 300 s (see Figure 10) which is probably due to the underestimation of accretion rate. Because the benchmark results shift to larger values, the ESM-like simulations based on different parameterization become biased low. Interestingly, as a result of error compensation, the performance of Liu2007 becomes better for $dt_{ESM}\Delta t$ = 1200 s. When all three major sources of uncertainty are considered, the ESM-like simulations slightly underestimate the benchmark results with an overall uncertainty within a factor of 4.

4. Summary and discussions

In this study we evaluated the performance of several bulk parameterization schemes for the simulation of warm rain in ESMs. A unique feature of this study is to use the extensive horizontal flight legs from an airborne measurement field campaign, ACE-ENA, to emulate a typical ESM grid. This enables us to obtain a comprehensive understanding of the performance of the parameterization schemes in ESM-like application scenarios. In contrast to previous evaluation studies that focused only on the simulation of local and instantaneous rates, our study considered the additional impacts of subgrid cloud spatial inhomogeneity and temporal averaging due to the

Accepted for publication in *Journal of the Atmospheric Sciences.* DOI 10.1175/JAS-D-23-0198.1.

large time step of ESM on the warm rain simulation. The main findings from this study include the following points:

- There is a large discrepancy between different autoconversion parameterization schemes for the simulation of grid-mean instantaneous autoconversion rates, indicating the dominance of parameterization uncertainty in the autoconversion simulation. Among the five autoconversion parameterization schemes evaluated, the KK2000 and Chiu2021 schemes based on numerical fitting perform better when the benchmark grid-mean instantaneous autoconversion rates are larger than 10^{-10} s^{-1}. For smaller autoconversion rates the modified KK2000 scheme is better. We emphasize that these calculations reflect the uncertainty of the various parameterizations themselves, since the autoconversion (and also accretion) rates are calculated locally and instantaneously and do not take into account subgrid variations.
- The two accretion schemes evaluated, KK2000 and Chiu2021, have a similar accuracy and both agree very well with the benchmark grid-mean instantaneous accretion rates.
- As described by Jessen's inequality, the subgrid variations of cloud and precipitation properties lead to a systematic underestimate of the autoconversion and accretion rates. This effect impacts the two semi-analytical schemes, Liu2007 and SB2001, more than the other schemes. But the underestimation errors due to Jessen's inequality partly compensate the overestimation tendency associated with these schemes, leading to an overall improvement for the simulation of grid-mean instantaneous autoconversion rates if the grid-mean cloud and precipitation properties are used in their parameterization calculation instead of the subgrid local values. For the KK2000 and Chiu2021 schemes, Jessen's inequality affects their autoconversion and accretion schemes to a similar extent despite the higher nonlinearity of the autoconversion formulae.
- The SCE-simulated total rain tendency due to the combined effects of autoconversion and accretion becomes increasingly nonlinear as the integration time increases from dt_{ESM} =300 s to the typical ESM time step size of dt_{ESM} = 1200s.
- After considering all the sources of uncertainty, the rain water tendencies simulated by the bulk parameterization schemes are mostly within a factor of 2 with the SCE benchmark results for dt_{ESM} =300 s. The uncertainty increases to a factor of 4 for dt_{ESM} =1200 s.

Accepted for publication in *Journal of the Atmospheric Sciences.* DOI 10.1175/JAS-D-23-0198.1.

It is interesting and important to note that there is not a single bulk parameterization scheme that performed significantly better than all other schemes when considering performance across all the hlegs and the three different classes of uncertainty. For example, even though the KK2000 and Chiu2021 schemes performed better for most hlegs for the local and instantaneous rate simulations, they tend to overestimate the very weak autoconversion which might have important implications for the simulation of warm rain in highly polluted regions. Moreover, the nonlinearity effects caused by subgrid spatial and sub-timestep temporal heterogeneity lead to an overall underestimation of these two schemes. On the other hand, it should also be noted that sometimes a good performance might be a result of error compensation.

Finally, it is important to point out a few limitations of this study. First, this study is based on the in-situ measurement from a single airborne field campaign. Its representativeness needs to be further evaluated by future studies based on more diverse data. Second, as pointed out in Section 2, the two semi-analytical parameterization schemes, SB2001 and Liu2007, were developed for certain DSD shapes. The comparisons presented in this study are based on the realistic and discrete DSDs, and therefore not completely fair to the semi-analytical schemes. Similarly, the Chiu2021 scheme used in this study is a highly simplified version from a more advanced machine-learning scheme without an explicit formula; the full capability of the ML-based Chiu2021 scheme is yet to be explored. Third, the warm rain parameterization schemes would interact with other components and processes in the ESM. For example, once the rain water is developed from the autoconversion and accretion, the sedimentation process would start to remove it, which would in turn affect the accretion process in the next time step. Such interactions are not considered in this study due to the limited scope. A few recent modeling studies investigated the time scales over which the bulk microphysics schemes are numerically sable and how the coupling of different microphysical processes is affected by the time integration in the ESMs (Santos et al. 2020, 2021). In the future, it would be interesting to put the findings from these modeling studies in the observation context.

Accepted for publication in *Journal of the Atmospheric Sciences.* DOI 10.1175/JAS-D-23-0198.1.

Acknowledgement:

We would like to acknowledge Dr. Johannes Mülmenstädt and the other anonymous reviewer for their insightful and suggestive comments which helped us improve this study significantly. Z. Zhang acknowledges the financial support from the Atmospheric System Research (Grant DE-SC0020057) funded by the Office of Biological and Environmental Research in the US Department of Energy Office of Science. Coauthor D. Mechem was supported by subcontract OFED0010-01 from the University of Maryland Baltimore County and the U.S. Department of Energy's Atmospheric Systems Research Grant No. DE-SC0023083. C. Chiu was supported by ASR, the Office of Science (BER), DOE under Grants DE-SC0021167. The computations in this study were performed at the UMBC High Performance Computing Facility. The facility is supported by the U.S. National Science Foundation through the MRI program (Grants CNS-0821258 and CNS-1228778) and the SCREMS program (Grant DMS-0821311), with substantial support from UMBC.

Accepted for publication in *Journal of the Atmospheric Sciences.* DOI 10.1175/JAS-D-23-0198.1.

Data and Software Availability

The Bott (1998) explicit bin model is archived at https://doi.org/10.5281/zenodo.5660185 (GNU Affero General Public License v3 or later). The FCDP data from ACE-ENA field campaign are publicly available from DOE Atmospheric Radiation Measurement (ARM) data center https://adc.arm.gov/discovery/#/results/id::6747_fcdp_micro_fcdp-air_airborne_cldpartsizedistr?showDetails=true. The 2D-s data from ACE-ENA field campaign are publicly available from ARM data center https://adc.arm.gov/discovery/#/results/id::6747_2ds_probe_sfcmet_2ds-air_cloud_hydrometsizedist?showDetails=true.

Accepted for publication in *Journal of the Atmospheric Sciences.* DOI 10.1175/JAS-D-23-0198.1.

References:

Albrecht, B. A., 1989: Aerosols, Cloud Microphysics, and Fractional Cloudiness. Science, 245, 1227–1230, https://doi.org/10.1126/science.245.4923.1227.

Bott, A., 1998: A Flux Method for the Numerical Solution of the Stochastic Collection Equation. *J Atmos Sci*, **55**, 2284–2293, https://doi.org/10.1175/1520-0469(1998)055<2284:afmftn>2.0.co;2.

Boutle, I. A., S. J. Abel, P. G. Hill, and C. J. Morcrette, 2014: Spatial variability of liquid cloud and rain: observations and microphysical effects. *Q J Roy Meteor Soc*, **140**, 583–594, https://doi.org/10.1002/qj.2140.

Covert, J. A., D. B. Mechem, and Z. Zhang, 2021: Subgrid-scale horizontal and vertical variation of cloud water in stratocumulus clouds: a case study based on LES and comparisons with in situ observations. *Atmos Chem Phys*, **22**, 1159–1174, https://doi.org/10.5194/acp-22-1159-2022.

Fan, J., Y. Wang, D. Rosenfeld, and X. Liu, 2016: Review of Aerosol–Cloud Interactions: Mechanisms, Significance, and Challenges. J Atmos Sci, 73, 4221–4252, https://doi.org/10.1175/jas-d-16-0037.1.

Gettelman, A., H. Morrison, C. R. Terai, and R. Wood, 2013: Microphysical process rates and global aerosol–cloud interactions. *Atmos Chem Phys*, **13**, 9855–9867, https://doi.org/10.5194/acp-13-9855-2013.

Gettelman, A., and H. Morrison, 2015: Advanced Two-Moment Bulk Microphysics for Global Models. Part I: Off-Line Tests and Comparison with Other Schemes. *J Climate*, **28**, 1268–1287, https://doi.org/10.1175/jcli-d-14-00102.1.

Accepted for publication in *Journal of the Atmospheric Sciences*. DOI 10.1175/JAS-D-23-0198.1.

Gettelman, A., Hannay, C., Bacmeister, J. T., Neale, R. B., Pendergrass, A. G., Danabasoglu, G., et al. 2019: High climate sensitivity in the Community Earth System Model version 2 (CESM2). Geophysical Research Letters, 46(14), 8329–8337. https://doi. org/10.1029/2019GL083978

Gettelman, A., D. J. Gagne, C. -C. Chen, M. W. Christensen, Z. J. Lebo, H. Morrison, and G. Gantos, 2021: Machine Learning the Warm Rain Process. *J Adv Model Earth Sy*, **13**, https://doi.org/10.1029/2020ms002268.

Gerber, H., G. Frick, S. Malinowski, J. Brenguier, and F. Burnet, 2005: Holes and entrainment in stratocumulus. J Atmos Sci, 62, 443–459, https://doi.org/10.1175/jas-3399.1.

Glienke, S., A. Kostinski, J. Fugal, R. A. Shaw, S. Borrmann, and J. Stith (2017), Cloud droplets to drizzle: Contribution of transition drops to microphysical and optical properties of marine stratocumulus clouds, Geophys. Res. Lett., 44, 8002–8010, doi:10.1002/ 2017GL074430.

Hsieh, W. C., H. Jonsson, L. -P. Wang, G. Buzorius, R. C. Flagan, J. H. Seinfeld, and A. Nenes, 2009: On the representation of droplet coalescence and autoconversion: Evaluation using ambient cloud droplet size distributions. *J Geophys Res Atmospheres*, **114**, https://doi.org/10.1029/2008jd010502.

Igel, A. L., 2019: Using an Arbitrary Moment Predictor to Investigate the Optimal Choice of Prognostic Moments in Bulk Cloud Microphysics Schemes. *J. Adv. Model. Earth Syst.*, **11**, 4559–4575, https://doi.org/10.1029/2019ms001733.

Jing, X., K. Suzuki, H. Guo, D. Goto, T. Ogura, T. Koshiro, and J. Mülmenstädt, 2017: A Multimodel Study on Warm Precipitation Biases in Global Models Compared to Satellite Observations. *J Geophys Res Atmospheres*, **122**, 11,806-11,824, https://doi.org/10.1002/2017jd027310.

Jing, X., K. Suzuki, and T. Michibata, 2019: The Key Role of Warm Rain Parameterization in Determining the Aerosol Indirect Effect in a Global Climate Model The Key Role of Warm Rain

Accepted for publication in *Journal of the Atmospheric Sciences*. DOI 10.1175/JAS-D-23-0198.1.

Parameterization in Determining the Aerosol Indirect Effect in a Global Climate Model. *J Climate*, **32**, 4409–4430, https://doi.org/10.1175/jcli-d-18-0789.1.

Khain, A. P., Beheng, K. D., Heymsfield, A., Korolev, A., Krichak, S. O., Levin, Z., Pinsky, M., Phillips, V., Prabhakaran, T., Teller, A., et al. (2015), Representation of microphysical processes in cloud-resolving models: Spectral (bin) microphysics versus bulk parameterization, Rev. Geophys., 53, 247– 322. doi:10.1002/2014RG000468.

Khairoutdinov, M., & Kogan, Y. (2000). A new cloud physics parameterization in a large-eddy simulation model of marine stratocumulus. *Monthly Weather Review*, *128*, 229–243.

Klein, S. A., and D. L. Hartmann, 1993: The Seasonal Cycle of Low Stratiform Clouds. J Climate, 6, 1587–1606, https://doi.org/10.1175/1520-0442(1993)006<1587:tscols>2.0.co;2.

Larson, V. E., and B. M. Griffin, 2013: Analytic upscaling of a local microphysics scheme. Part I: Derivation. Q J Roy Meteor Soc, 139, 46–57, https://doi.org/10.1002/qj.1967.

Lau, K. M., and H. T. Wu, 2003: Warm rain processes over tropical oceans and climate implications. Geophys Res Lett, 30, https://doi.org/10.1029/2003gl018567.

Lebsock, M., H. Morrison, and A. Gettelman, 2013: Microphysical implications of cloud-precipitation covariance derived from satellite remote sensing. *J Geophys Res Atmospheres*, **118**, 6521–6533, https://doi.org/10.1002/jgrd.50347.

L'Ecuyer, T. S., W. Berg, J. Haynes, M. Lebsock, and T. Takemura, 2009: Global observations of aerosol impacts on precipitation occurrence in warm maritime clouds. *J. Geophys. Res.*, **114**, D09211, doi:10.1029/2008JD011273.

Liu, Y., P. H. Daum, and R. McGraw (2004), An analytical expression forpredicting the critical radius in the autoconversion parameterization, *Geophys. Res. Lett.*, *31*, L06121, doi:10.1029/2003GL019117.

Accepted for publication in *Journal of the Atmospheric Sciences*. DOI 10.1175/JAS-D-23-0198.1.

Liu, Y., P. H. Daum, and R. McGraw (2005), Size truncation effect, thresh-old behavior, and a new type of autoconversion parameterization, *Geophys. Res. Lett*., *32*, L11811, doi:10.1029/2005GL022636.

Liu, Y., P. H. Daum, and R. McGraw (2006a), Parameterization of theautoconversion process. part II: Generalization of Sundqvist-type para-meterizations, *J. Atmos. Sci*., *63*, 1103–1109.

Liu, Y., P. H. Daum, R. McGraw, and M. Miller (2006b), Generalizedthreshold function accounting for effect of relative dispersion on thresh-old behavior of autoconversion process, *Geophys. Res. Lett*., *33*, L11804,doi:10.1029/2005GL025500.

Liu, Y., Daum, P. H., McGraw, R. L., Miller, M. A., & Niu, S. (2007). Theoretical expression for the autoconversion rate of the cloud droplet number concentration. *Geophysical research letters*, 34 (16).

Mei, Fan, and Brian Ermold. "Merged Data- Common Timestamp (AAFMERGEDCLDSD)." Atmospheric Radiation Measurement (ARM) user facility, n.d. Accessed May 29, 2023. https://doi.org/10.5439/1897918.

Morrison, H., and A. Gettelman, 2008: A New Two-Moment Bulk Stratiform Cloud Microphysics Scheme in the Community Atmosphere Model, Version 3 (CAM3). Part I: Description and Numerical Tests. *J Climate*, **21**, 3642–3659, https://doi.org/10.1175/2008jcli2105.1.

Mülmenstädt, J., O. Sourdeval,J. Delanoë, and J. Quaas (2015),Frequency of occurrence of rain fromliquid-, mixed-, and ice-phase cloudsderived from A-Train satellite retrievals,Geophys. Res. Lett.,42, 6502–6509,doi:10.1002/2015GL064604

Accepted for publication in *Journal of the Atmospheric Sciences*. DOI 10.1175/JAS-D-23-0198.1.

Mülmenstädt, J., and Coauthors, 2020: Reducing the aerosol forcing uncertainty using observational constraints on warm rain processes. *Sci Adv*, **6**, eaaz6433, https://doi.org/10.1126/sciadv.aaz6433.

Mülmenstädt, J., and Coauthors, 2021: An underestimated negative cloud feedback from cloud lifetime changes. *Nat Clim Change*, **11**, 508–513, https://doi.org/10.1038/s41558-021-01038-1.

Pincus, R., and S. A. Klein, 2000: Unresolved spatial variability and microphysical process rates in large-scale models. J Geophys Res Atmospheres, 105, 27059–27065, https://doi.org/10.1029/2000jd900504.

Pruppacher, H. R., and J. D. Klett, 1997: *Microphysics of Clouds and Precipitation*. 2nd ed. Kluwer Academic Publishers, 954 pp.

Rasch, P. J., Xie, S., Ma, P.-L., Lin, W., Wang, H., Tang, Q., Burrows, S. M., Caldwell, P., Zhang, K., Easter, R. C., et al. (2019), An Overview of the Atmospheric Component of the Energy Exascale Earth System Model, J. Adv. Model. Earth Syst., 11, 2377– 2411. doi:https://doi.org/10.1029/2019MS001629.

Rotstayn, L. D., 2000: On the "tuning" of autoconversion parameterizations in climate models. *J. Geophys. Res.: Atmos.*, **105**, 15495–15507, https://doi.org/10.1029/2000jd900129.

Seifert, A., and K. D. Beheng, 2001: A double-moment parameterization for simulating autoconversion, accretion and selfcollection. *Atmospheric Research*, **59–60**, 265–281.

Shima, S., K. Kusano, A. Kawano, T. Sugiyama, and S. Kawahara, 2009: The super-droplet method for the numerical simulation of clouds and precipitation: a particle-based and probabilistic microphysics model coupled with a non-hydrostatic model. Q J Roy Meteor Soc, 135, 1307–1320, https://doi.org/10.1002/qj.441.

Accepted for publication in *Journal of the Atmospheric Sciences*. DOI 10.1175/JAS-D-23-0198.1.

Santos, S. P., P. M. Caldwell, and C. S. Bretherton, 2020: Numerically Relevant Timescales in the MG2 Microphysics Model. *J. Adv. Model. Earth Syst.*, **12**, https://doi.org/10.1029/2019ms001972.

Santos, S. P., P. M. Caldwell, and C. S. Bretherton, 2021: Cloud Process Coupling and Time Integration in the E3SM Atmosphere Model. *J. Adv. Model. Earth Syst.*, **13**, https://doi.org/10.1029/2020ms002359.

Song, H., Z. Zhang, P.-L. Ma, S. Ghan, and M. Wang, 2018a: An Evaluation of Marine Boundary Layer Cloud Property Simulations in Community Atmosphere Model Using Satellite Observations: Conventional Sub-grid Parameterization vs. CLUBB. *J Climate*, **31**, 2299–2320, https://doi.org/10.1175/jcli-d-17-0277.1.

Song, H., Z. Zhang, P.-L. Ma, S. Ghan, and M. Wang, 2018b: The importance of considering sub-grid cloud variability when using satellite observations to evaluate the cloud and precipitation simulations in climate models. *Geosci Model Dev*, **11**, 3147–3158, https://doi.org/10.5194/gmd-11-3147-2018.

Stephens, G. L., and Coauthors, 2010: Dreary state of precipitation in global models. *J Geophys Res Atmospheres 1984 2012*, **115**, 1147, https://doi.org/10.1029/2010jd014532.

Suzuki, K., G. Stephens, A. Bodas-Salcedo, M. Wang, J.-C. Golaz, T. Yokohata, and T. Koshiro, 2015: Evaluation of the Warm Rain Formation Process in Global Models with Satellite Observations. *J Atmos Sci*, **72**, 150803130410002, https://doi.org/10.1175/jas-d-14-0265.1.

Twomey, S., 1977: The influence of pollution on the shortwave albedo of clouds. 34, 1149–1152.

Wang, J., and Coauthors, 2021: Aerosol and Cloud Experiments in the Eastern North Atlantic (ACE-ENA). *B Am Meteorol Soc*, 1–51, https://doi.org/10.1175/bams-d-19-0220.1.

Accepted for publication in *Journal of the Atmospheric Sciences*. DOI 10.1175/JAS-D-23-0198.1.

Wang, M., and Coauthors, 2012: Constraining cloud lifetime effects of aerosols using A-Train satellite observations. *Geophys Res Lett*, **39**, L15709, https://doi.org/10.1029/2012gl052204.

Weber, T., and J. Quaas, 2013: Incorporating the subgrid-scale variability of clouds in the autoconversion parameterization using a PDF-scheme. *J. Adv. Model. Earth Syst.*, **4**, https://doi.org/10.1029/2012ms000156.

Wood, R., 2005a: Drizzle in Stratiform Boundary Layer Clouds. Part I: Vertical and Horizontal Structure. J Atmos Sci, 62, 3011–3033, https://doi.org/10.1175/jas3529.1.

Wood, R., 2005b: Drizzle in Stratiform Boundary Layer Clouds. Part II: Microphysical Aspects. J Atmos Sci, 62, 3034–3050, https://doi.org/10.1175/jas3530.1.

Wood, R., C. Bretherton, D. Leon, A. Clarke, P. Zuidema, G. Allen, and H. Coe, 2011: An aircraft case study of the spatial transition from closed to open mesoscale cellular convection over the southeast Pacific. Atmos. Chem. Phys., 11, 2341–2370.

Wood, R., 2012: Stratocumulus Clouds. Mon Weather Rev, 140, 2373–2423, https://doi.org/10.1175/mwr-d-11-00121.1.

Yu, S., and M. S. Pritchard, 2015: The effect of large-scale model time step and multiscale coupling frequency on cloud climatology, vertical structure, and rainfall extremes in a superparameterized GCM. *J. Adv. Model. Earth Syst.*, **7**, 1977–1996, https://doi.org/10.1002/2015ms000493.

Zhang, Z., H. Song, P.-L. Ma, V. E. Larson, M. Wang, X. Dong, and J. Wang, 2019: Subgrid variations of the cloud water and droplet number concentration over the tropical ocean: satellite observations and implications for warm rain simulations in climate models. *Atmos Chem Phys*, **19**, 1077–1096, https://doi.org/10.5194/acp-19-1077-2019.

Accepted for publication in *Journal of the Atmospheric Sciences*. DOI 10.1175/JAS-D-23-0198.1.

Zhang, Z., and Coauthors, 2021: Vertical dependence of horizontal variation of cloud microphysics: observations from the ACE-ENA field campaign and implications for warm-rain simulation in climate models. *Atmos Chem Phys*, **21**, 3103–3121, https://doi.org/10.5194/acp-21-3103-2021.

Zhang, Z., L. Oreopoulos, M. D. Lebsock, D. B. Mechem, and J. Covert, 2022: Understanding the microphysical control and spatial-temporal variability of warm rain probability using CloudSat and MODIS observations. Geophys Res Lett, https://doi.org/10.1029/2022gl098863.

Accepted for publication in *Journal of the Atmospheric Sciences.* DOI 10.1175/JAS-D-23-0198.1.